

Reservoir Computing with Error Correction: Long-term Behaviors of Stochastic Dynamical Systems

Cheng Fang ^{*a}, Yubin Lu ^{†b}, Ting Gao ^{‡a}, and Jinqiao Duan ^{§c}

^aSchool of Mathematics and Statistics & Center for Mathematical Sciences, Huazhong University of Science and Technology, Wuhan, Hubei 430074, China

^bDepartment of Applied Mathematics, College of Computing, Illinois Institute of Technology, Chicago, IL 60616, USA

^cDepartment of Mathematics and Department of Physics, Great Bay University, Dongguan, Guangdong 523000, China

May 2, 2023

Abstract

The prediction of stochastic dynamical systems and the capture of dynamical behaviors are profound problems. In this article, we propose a data-driven framework combining Reservoir Computing and Normalizing Flow to study this issue, which mimics error modeling to improve the traditional Reservoir Computing performance and takes advantage of both approaches. This model-free method successfully predicts the long-term evolution of stochastic dynamical systems and replicates dynamical behaviors. With few assumptions about the underlying stochastic dynamical systems, we deal with Markov/non-Markov and stationary/non-stationary stochastic processes defined by linear/nonlinear stochastic differential equations or stochastic delay differential equations. We verify the effectiveness of the proposed framework in five experiments, including the Ornstein-Uhlenbeck process, Double-Well system, El Niño Southern Oscillation simplified model, and stochastic Lorenz system. Additionally, we explore the noise-induced tipping phenomena and the replication of the strange attractor.

Keywords: Stochastic dynamical system, Stochastic delay differential equation, Reservoir Computing, Normalizing Flow, Dynamical behaviors.

1 Introduction

Stochastic dynamical systems describe the evolution of complex phenomena in the presence of noise. This noise may arise from a range of factors such as external fluctuations, internal agitation, uncertainty in initial/boundary conditions and parameters. The interplay between deterministic governing laws and noise results in corresponding stochastic dynamical behaviors. For example, stochastic (delay) differential equations (SDEs/SDDEs) [1–3] are two significant mathematical models that accurately describe the evolution of deterministic dynamical systems in the presence of noise. These models have demonstrated successful applications in various fields, including biology, chemistry, physics, and meteorology [1, 3–5].

For a given dynamical system, what we are concerned about are not only the state of the system, but also the dynamical behaviors it exhibits. Practical problems are usually complex and difficult to be described by concise mathematical models. As a result, their corresponding dynamical systems can be so complex that are difficult to solve. Therefore, one of the main strategies to study dynamical systems is to design appropriate tools that can characterize their behaviors, rather than solving them

*fangcheng1@hust.edu.cn

†Corresponding author: ylu117@iit.edu

‡tgao0716@hust.edu.cn

§duan@gbu.edu.cn

directly. Over the past century, researchers have developed various kinds of qualitative methods to characterize dynamical systems, such as bifurcations, chaos, attractors and their fractal dimensions [6]. Furthermore, the dynamical behaviors of stochastic dynamical systems are richer and more challenging to quantify and analyze due to the impact of noise. For instance, for a multistable dynamical system, when noise is present, the state variable stays close to a metastable equilibrium for a long time and may sometimes cross the unstable manifold and fall into the basin of attraction of another metastability. This phenomenon is also a kind of noise-induced tipping [7].

In spite of this principle-based research paradigm, one may encounter complex phenomena that lack sufficient scientific understanding. While it may not be possible to establish a complete mathematical model for highly complex phenomena, the ever-advancing fields of computer technology and observation techniques have made the data-driven research paradigm not only possible but also flourishing. In the last ten to twenty years, many data-driven methods for studying stochastic dynamical systems have been proposed and have shown a thriving development in various fields. For example, extracting stochastic governing laws from data by Koopman operators [8, 9], Kramers-Moyal formulas [10, 11], maximum likelihood estimations [12, 13], physics-informed neural networks [14, 15], or estimating the probability distribution for the corresponding stochastic dynamical system [16]. Methods developed in the area of deep learning for analyzing time series are also used to study stochastic dynamical systems, for instance, forecasting the evolution of stochastic dynamical systems by Recurrent Neural Networks (RNN) [17], Neural SDE [18], or statistics-informed neural networks [19], and discovering the dynamical behavior from data [17, 19].

The term ‘‘Reservoir Computing’’ (RC) [20] refers to a broad computational framework derived from RNN, which was developed by Jaeger [21] and Maass et al. [22, 23]. These papers, in turn, introduced the ideas of Echo State Networks (ESN) and Liquid State Machines (LSM), respectively. The benefits of RC include its simple structure, easy training, and fixed reservoirs, which also make it effective for large-scale or high-dimensional datasets. RC has exhibited strong prediction capabilities that can guarantee prediction accuracy over a long period of time for chaotic systems [21, 24–27]. When concentrating on the dynamical behaviors of dynamical systems, RC replicates strange attractors, the basin of attraction, stable/unstable manifolds, etc [25, 26, 28–30]. This method has been employed with success for more challenging tipping and critical transition phenomena in dynamical systems [31–33]. As for its interpretability, the properties, the structure of its latent representation and the universality are also in progress [26, 34–37]. Several new architectures of RC are being developed [27, 29, 38]. Physical RC, another branch of the RC research field, refers to hardware implementation using various physical systems, substrates, and devices [39]. Besides, there are few studies utilizing RC for dynamical systems with noise, which is discussed in detail in Sec. 2.2.

Reservoir computing has manifested powerful approximation capabilities for deterministic dynamical systems, but due to the lack of an effective stochastic structure, it is still insufficient for stochastic dynamical systems. In other words, proper probabilistic modeling of errors is a key aspect in dealing with stochastic dynamical systems [17, 40, 41]. Fortunately, the probabilistic generative models in the machine learning community are flourishing and have shown effective approximation capabilities for high-dimensional and complex probability distributions. The most popular models in recent years include Generative Adversarial Networks (GANs) [42], Variational Auto-Encoders (VAEs) [43], Diffusion Models (DMs) [44] and Normalizing Flows (NFs) [11, 16, 45–47], which have been successfully applied in areas such as image generation and speech synthesis.

Reservoir computing is an effective approximator for deterministic dynamical systems, while probabilistic generative models are designed to learn the underlying probability distribution of a dataset. Inspired by this, we combine Reservoir Computing and Normalizing Flow (RC-NF for short) to realize long-term prediction of stochastic dynamical systems and capture various dynamical behaviors of stochastic dynamical systems. This framework is model-free and imposes fewer constraints on the studied system. The main contributions of this work include:

- Methodological innovation: the improved RC method (i.e., RC-NF introduced below) is successfully applied in stochastic dynamical systems, both defined by stochastic differential equations and stochastic delay differential equations, which can be extended to more complex stochastic systems;
- Robustness: we successfully predict the long-term evolution of stochastic dynamical systems, including linear/non-linear systems, Markov/non-Markov processes, and stationary/non-stationary models;

- Dynamical behaviors characterization: we successfully capture the dynamical behaviors of stochastic dynamical systems, such as noise-induced tipping and chaos. For stochastic chaotic systems, RC-NF is more effective than traditional RC.

From a theoretical perspective, we also demonstrate the universality of RC-NF. We further illustrate the effectiveness of the approach using criteria such as Wasserstein distance, Kullback-Leibler divergence, transition rate, maximum Lyapunov exponent, close returns, autocorrelation function, and cross-correlation function in different experiments.

The remainder of this article is arranged as follows: Sec. 2 introduces stochastic dynamical systems defined by stochastic (delay) differential equations, related works, and unresolved issues. In Sec. 3, we begin by presenting the general frameworks of reservoir computing and normalizing flow. We then combine these frameworks to analyze stochastic dynamical systems using data. At the end of this section, a thorough analysis of the approximation ability is provided. In Sec. 4, we demonstrate the effectiveness of our method through validation on a variety of examples, including the Ornstein–Uhlenbeck process, Double-Well system, linear SDDE, El Niño Southern Oscillation simplified model, and stochastic Lorenz system. In Sec. 5, we discuss our findings and potential directions for improving this work.

2 Preliminary works

In this section, we briefly introduce stochastic dynamical systems and highlight some related data-driven approaches that have been applied to them. Based on this, we point out the goals of this work. In the following, bold letters denote multidimensional vectors or random variables, while the subscript ‘t’ indicates time (continuous or discrete, depending on the context). The superscript ‘i’ represents different dimensions, and the superscript ‘(m)’ denotes different sample trajectories, unless otherwise specified.

2.1 Stochastic dynamical systems

Stochastic differential equations and stochastic delay differential equations are two types of models with significantly different characteristics. One of the key differences between the two is that the solutions of the former are Markov processes, but the solutions of the latter are typically non-Markov processes. This makes it difficult for general data-driven models to handle both types of systems simultaneously.

• Stochastic differential equations

We consider the following stochastic dynamical systems defined by stochastic differential equations (SDEs) in \mathbb{R}^d [1]:

$$d\mathbf{X}_t = \mathbf{f}(\mathbf{X}_t)dt + \mathbf{g}(\mathbf{X}_t)d\mathbf{B}_t, \quad (1)$$

where $t \in \mathbb{R}^+$, $\mathbf{X}_t = [X_t^1, X_t^2, \dots, X_t^d]^T \in \mathbb{R}^d$ (the superscript T stands for transpose of a vector or a matrix), the drift coefficient $\mathbf{f}(\mathbf{X}_t) \in \mathbb{R}^d$ and the noise intensity (or diffusion coefficient matrix) $\mathbf{g}(\mathbf{X}_t) \in \mathbb{R}^d \times \mathbb{R}^d$. In this article, we assume that $\mathbf{g}(\mathbf{X}_t)$ is a diagonal matrix and that the elements on the diagonal are constants. A discussion of $\mathbf{g}(\mathbf{X}_t)$ as a non-diagonal matrix can be found in [13]. The Brownian motion \mathbf{B}_t , taking values in \mathbb{R}^d , is a Gaussian process on an underlying probability space (Ω, \mathcal{F}, P) . More specifically, the stochastic process \mathbf{B}_t satisfies: (a) $\mathbf{B}_0 = \mathbf{0}$, a.s.; (b) \mathbf{B}_t has continuous paths, a.s.; (c) \mathbf{B}_t has independent and stationary increments, and $\mathbf{B}_t - \mathbf{B}_s \sim N(\mathbf{0}, (t-s)\mathbf{I})$, for $t > s \geq 0$, where N represents Gaussian distribution and \mathbf{I} is the $d \times d$ identity matrix. Moreover, we should notice that the solution \mathbf{X}_t of (1) is a Markov process.

It is well known that the probability density function for a given SDE satisfies a Fokker-Planck equation. That is, the probability density function p for the SDE (1) satisfies

$$\frac{\partial}{\partial t} p(x, t) = A^* p(x, t), \quad (2)$$

where A^* is often called the Fokker-Planck operator, $A^* p = -\sum_{i=1}^d \frac{\partial}{\partial x_i} (f_i p) + \frac{1}{2} \sum_{i,j=1}^d \frac{\partial^2}{\partial x_i \partial x_j} ((g g^T)_{ij} p)$.

• Stochastic delay differential equations

Stochastic delay differential equations (SDDEs) are appropriate models for describing stochastic dynamical systems with memory. A stochastic delay differential equation with delay τ in \mathbb{R}^d is described

by

$$\begin{cases} d\mathbf{X}_t = \mathbf{f}(\mathbf{X}_t, \mathbf{X}_{t-\tau})dt + \mathbf{g}(\mathbf{X}_t, \mathbf{X}_{t-\tau})d\mathbf{B}_t & \text{for } t > 0, \\ \mathbf{X}_t = \boldsymbol{\gamma}_{-t} & \text{for } t \in [-\tau, 0], \end{cases} \quad (3)$$

where $\tau \in \mathbb{R}^+$ is time delay, $\boldsymbol{\gamma} : [0, \tau] \rightarrow \mathbb{R}^d$, $\mathbf{f} : \mathbb{R}^d \times \mathbb{R}^d \rightarrow \mathbb{R}^d$, $\mathbf{g} : \mathbb{R}^d \times \mathbb{R}^d \rightarrow \mathbb{R}^d$. The non-Markov property resulting from delays makes it challenging to obtain governing equations for probability densities associated with SDDEs. Despite this, as demonstrated below, our framework is suitable for stochastic dynamical systems induced by SDDEs.

Based on the theory of stochastic analysis, powerful mathematical tools have been developed for the study of stochastic dynamical systems. However, due to the existence of randomness, many analytical tasks have become particularly challenging. For example, there are fewer examples of stochastic differential equations that can be solved explicitly compared to ordinary differential equations, and the definition of the dynamical behavior of stochastic dynamical systems is more complex. Therefore, it is necessary to develop data-driven methods for analyzing stochastic dynamical systems, especially for studies that can simultaneously handle both SDEs and SDDEs.

2.2 Related works and unresolved issues

Various data-driven approaches have been proposed for the analysis of stochastic dynamical systems. However, most existing works heavily rely on specific model assumptions. For instance, the methods utilizing the Koopman operator [8, 9] or Kramers-Moyal formulas [10, 11] necessitate the assumption that the systems under study are stochastic differential equations. Maximum likelihood estimations [12, 13] are constructed based on numerical schemes of stochastic differential equations. The physics-informed neural network used to learn stochastic dynamical systems typically presupposes the presence of the Fokker-Planck equation [14, 15]. In other words, these methods overly rely on assumptions of the model, which limits their extension. These methods are not applicable to SDDEs, which serves as a concrete example.

As a type of Recurrent Neural Network, Reservoir Computing is a model-free method that can be directly applied to time series modeling, while its structure is simpler than other methods [17–19]. Moreover, it has demonstrated strong approximation capabilities for deterministic dynamical systems, regardless of the presence of time-delay effects. Therefore, it has the potential to become a powerful tool for studying stochastic dynamical systems. There are a few applications of RC for stochastic systems. For example, the effect of stochasticity is also addressed in [32, 33]. They assume the noise originates from observations and obeys a uniform distribution. However, the randomness is treated as external noise. SDEs or SDDEs defined in Sec. 2.1 treat the randomness as intrinsic noise and are more widely studied. Moreover, the systems studied in [32, 33] have similar dynamical behaviors (eg., intermittency, chaos) whether noise is present or not. While the systems we studied show significantly different dynamical behaviors compared to their deterministic counterparts since the noise is treated as an intrinsic part. In [31], authors investigate stochastic systems and select a specific trajectory with constraints for training, while our method works on trajectory data without these constraints. Besides, in [48], authors use RC to study the stochasticity caused by numerical schemes for determining systems. The method mentioned in [49] requires the cooperation of physical hardware to realize the mask of data on stochastic resonance systems. In contrast, we directly use trajectories of stochastic dynamical systems without mask operations.

The primary objective of this study is to propose a novel method to make long-term predictions regarding the evolution of stochastic dynamical systems. To be more precise, the aim is to use finite-length trajectories generated or observed from a stochastic process in order to predict probability distributions consisting of predicted trajectories in future instances. Not only can the trained model generate trajectories, but it can also predict the dynamical behaviors of stochastic dynamical systems, including transitions between metastabilities, noise-induced tipplings, strange attractors, and more.

3 Data-driven forecasting for stochastic dynamical systems

Stochastic dynamical systems induced by stochastic differential equations or stochastic delay differential equations could exhibit extremely different dynamical behaviors, such as converging to an equilibrium distribution, transition between metastable states, time-delay behavior, and chaotic behavior. In

order to predict the future states or capture the dynamical behavior of a stochastic dynamical system from observed time series data, we combine Reservoir Computing and a deep generative model (e.g., Normalizing Flow) to establish a unified framework for forecasting long-term evolution and capturing the dynamical behavior. In Sec. 3.1, we briefly introduce the general description of Reservoir Computing. In Sec. 3.2, we present how to compensate for the approximated errors coming from the surrogate model (Reservoir Computing). In Sec. 3.3, we illustrate how to combine these two key ingredients (Reservoir Computing and Normalizing Flow) for studying stochastic dynamical systems. In Sec. 3.4, we analyze the universality of the proposed approach.

3.1 Reservoir Computing for long-term forecasting

The umbrella term called Reservoir Computing (RC) is a type of Recurrent Neural Network, which is well known for its long prediction time, few training parameters, and low computational cost. We provide an outline framework of Reservoir Computing as follows.

Consider a time-discrete stochastic dynamical system (1) or (3) $\{\mathbf{X}_t\}_{t=0}^{T-1}$, where $\mathbf{X}_t \in \mathbb{R}^d$ and T is the length of time series. The time step size is denoted by Δt . Assume that the reservoir has N nodes, then the d dimension input vector at each iteration is coupled into the reservoir via an $N \times d$ dimensional input-to-reservoir coupling matrix W_{in} . We construct this matrix by randomly sampling each matrix element from a uniform distribution on the interval $[-\chi, \chi]$. The state of the reservoir at time t is denoted by the N dimensional vector $\mathbf{r}_t = [r_t^1, r_t^2, \dots, r_t^N]^T$. The time evolution of the reservoir state \mathbf{r}_t is determined by [20]

$$\mathbf{r}_{t+1} = (1 - \alpha)\mathbf{r}_t + \alpha \tanh(A\mathbf{r}_t + W_{in}\mathbf{X}_t + \boldsymbol{\zeta}), \quad (4)$$

when $\Delta t \rightarrow 0$, equation (4) can be approximated as

$$\dot{\mathbf{r}}_t \approx \frac{\mathbf{r}_{t+1} - \mathbf{r}_t}{\Delta t} = -\frac{\alpha}{\Delta t}\mathbf{r}_t + \frac{\alpha}{\Delta t} \tanh(A\mathbf{r}_t + W_{in}\mathbf{X}_t + \boldsymbol{\zeta}), \quad (5)$$

where A (an $N \times N$ matrix) is the adjacency matrix of the reservoir, α defines the leakage factor, the hyperbolic tangent function is applied element-wise to the vector, and the vector $\boldsymbol{\zeta} := \mathbf{w}_{in}^T \cdot \mathbf{1} \in \mathbb{R}^N$ where elements of \mathbf{w}_{in} also sample from the uniform distribution on the interval $[-\chi, \chi]$. The initial condition for the hidden state can be conveniently set to be $\mathbf{r}(t=0) = \mathbf{0}$. The adjacency matrix A defines a random network of size N and average degree $\langle k \rangle$. Here, the average degree $\langle k \rangle$ of a network is the average number of links that a node has. Furthermore, matrix A is rescaled such that the spectral radius of the network is ρ . The spectral radius ρ of a network is the largest absolute value of the eigenvalues of its adjacency matrix. An intriguing and significant aspect of RC is that, once the aforementioned matrices A , W_{in} and vector $\boldsymbol{\zeta}$ are created, they are never trained and are always fixed. This means that input vectors enter the reservoir in a fixed manner and that the connections between neurons within the reservoir do not change.

The input sequence and the desired output sequence in our work are essentially products of the same system and share the same dimension (for more general tasks, they are inconsistent). Subsequently, using a readout matrix, the estimation of RC at time $t+1$ is obtained,

$$\hat{\mathbf{X}}_{t+1} = W_{out}[1; \mathbf{X}_t; \mathbf{r}_{t+1}]^T, \quad (6)$$

where output layer W_{out} is a $d \times (1 + d + N)$ matrix with trainable weights. By minimizing the \mathcal{L}_2 error between the target states \mathbf{X}_t and the estimate states $\hat{\mathbf{X}}_t = W_{out}[1; \mathbf{X}_t; \mathbf{r}_{t+1}]^T$, the matrix W_{out} is trained. More specifically, the loss function is

$$\mathcal{L}_{RC} = \sum_{t=1}^{T-1} \|\hat{\mathbf{X}}_t - \mathbf{X}_t\|^2 + \lambda \|W_{out}\|^2, \quad (7)$$

where $\lambda > 0$ is the regularization hyperparameter, the term $\lambda \|W_{out}\|^2$ is added to prevent overfitting. Using the Tikhonov transformation, also called ridge regression, the above loss function (7) can be solved in closed form:

$$W_{out} = \mathbf{Y}\mathbf{R}^T(\mathbf{R}\mathbf{R}^T + \lambda\mathbf{I})^{-1}, \quad (8)$$

where \mathbf{R} is the states matrix of dimension $(1 + d + n) \times (T - 1)$, built using combinations of column vectors $[1; \mathbf{X}_{t-1}; \mathbf{r}_t]^T$ for every $t = 1, \dots, T - 1$. The matrix \mathbf{Y} is built in the same way using \mathbf{X}_t , for $t = 1, \dots, T - 1$. \mathbf{I} is an identity matrix of dimension $1 + d + N$.

The prediction phase uses the same update equations as those above (eq. (4), (6)) after the matrix W_{out} obtained, but the input \mathbf{X}_t is represented by the calculated output $\hat{\mathbf{X}}_t$ of the preceding step.

The construction of the RC framework involves several hyperparameters, and in this article, we focus on the impact of five specific hyperparameters on RC: the spectral radius ρ and average degree $\langle k \rangle$ of adjacency matrix A ; the sampling range χ of elements of matrix W_{in} ; leakage factor α ; regularization parameter λ . Selecting suitable hyperparameters is crucial because the trainable component of RC is only readout matrix W_{out} , its fixed part is less malleable and therefore relies heavily on the appropriate choice of hyperparameters. The primary methods for hyperparameter tuning include grid search [50], gradient descent [34], and others.

Bayesian Optimization (BO) [24, 26, 51] is a sequential design strategy for global optimization of black-box functions that does not assume any functional forms. It is more effective than grid search and performs well with minimal tuning. At each iteration, the BO algorithm chooses a set of hyperparameters from a selectable range of hyperparameters based on the posterior distribution of a loss function. Exploit uncertainty to balance exploration against exploitation. Inspired by [24, 26, 51], we select the range of each hyperparameter as shown in Table 1, considering the efficiency of the algorithm and the reasonableness of the hyperparameters.

Table 1: The value range and data type of hyperparameters of RC in the Bayesian Optimization algorithm

Hyperparameters	Min - Max	Data type
ρ	0.3 - 1.5	Real number
k	1 - 5	Integer
χ	0.3 - 1.5	Real number
α	0.05 - 1	Real number
λ	$10^{-10} - 1$	Real number

3.2 Error modelling

It is a fundamental fact that when a model generates multi-step rolling predictions, errors can accumulate rapidly. However, for deterministic systems, reservoir computing can ensure a certain level of time prediction accuracy. For example, traditional Reservoir Computing has achieved 5–6 Lyapunov times in the prediction of large-scale spatiotemporal chaotic sequences [25]. The presence of stochasticity in dynamical systems renders Reservoir Computing alone inadequate for accurately predicting their long-term behavior (as seen in Sec. 4). Due to the rolling prediction characteristics of RC, we are inspired by Kalman filtering [40, 52] and error modeling [17, 41] to compensate for the performance of RC in stochastic systems. RC can be regarded as a surrogate model for the original system. After modeling the error between the two, a strategy similar to Kalman Filtering is used to correct the subsequent predictions. Unlike deterministic systems, given the inherently random nature of stochastic dynamical systems, it is appropriate to assess the accuracy of predictions in terms of their probability distributions.

For a trajectory of a stochastic dynamical system, the single-step error at time t between the RC prediction $\hat{\mathbf{X}}_t$ and true trajectory data \mathbf{X}_t is $\tilde{\epsilon}^{(m)} := \mathbf{X}_t^{(m)} - \hat{\mathbf{X}}_t^{(m)}$, where $m = 1, \dots, M$ represents M different trajectories from the same stochastic dynamical system. The notation $\mathbf{p}(\tilde{\epsilon})$ represents the probability density formed by error $\tilde{\epsilon} := \{\tilde{\epsilon}^{(m)}\}$, $\mu_{\tilde{\epsilon}}$ stands for its probability measure. Under appropriate assumptions (Assumption 1 in Sec. 3.4), we claim that the probability density $\mathbf{p}(\tilde{\epsilon})$ of the single-step error $\tilde{\epsilon}$ does not change with time. It might be a strong assumption, but we will see that it is reasonable for the studied systems below. Further exploration of this issue is left for future research. Various probabilistic generative models can be employed to estimate the probability distribution of the error $\tilde{\epsilon}$ from data including Generative Adversarial Networks [42], Variational Auto-Encoders [43], Diffusion Models [44] and Normalizing Flows [11, 16, 45–47]. Unlike high-dimensional data such as images, our work focuses primarily on lower-dimensional physical systems. Therefore, we

use Normalizing Flows to estimate the distribution of errors. However, we must point out that other probabilistic generative models may also be used here, but they do not have any essential differences.

The main idea of Normalizing Flow (NF) is to find an invertible, differentiable transformation mapping the target random variable $\tilde{\boldsymbol{\varepsilon}} \in \mathbb{R}^d$ to a base random variable $\mathbf{u} \in \mathbb{R}^d$:

$$\tilde{\boldsymbol{\varepsilon}} = \mathbf{h}_\theta^{-1}(\mathbf{u}) \quad \mathbf{u} = \mathbf{h}_\theta(\tilde{\boldsymbol{\varepsilon}}), \quad (9)$$

where the map $\mathbf{h}_\theta : \mathbb{R}^d \rightarrow \mathbb{R}^d$ is invertible, differentiable, and θ represents all parameters to be trained. The change of variables formula is that

$$\underbrace{\mathbf{p}(\tilde{\boldsymbol{\varepsilon}})}_{\text{over } \tilde{\boldsymbol{\varepsilon}}} = \underbrace{\mathbf{p}(\mathbf{h}_\theta(\tilde{\boldsymbol{\varepsilon}}))}_{\text{over } \mathbf{u}} \left| \det \left(\frac{\partial \mathbf{h}_\theta(\tilde{\boldsymbol{\varepsilon}})}{\partial \tilde{\boldsymbol{\varepsilon}}} \right) \right|, \quad (10)$$

where $\frac{\partial \mathbf{h}_\theta(\tilde{\boldsymbol{\varepsilon}})}{\partial \tilde{\boldsymbol{\varepsilon}}}$ denotes the $d \times d$ Jacobian matrix.

Usually, we select a simple distribution as the base distribution, $\mathbf{u} \sim N(\mathbf{0}, \mathbf{I})$. Suppose we compose k transformations $\mathbf{h}_\theta(\tilde{\boldsymbol{\varepsilon}}) = \mathbf{h}_1 \circ \mathbf{h}_2 \circ \dots \circ \mathbf{h}_k(\tilde{\boldsymbol{\varepsilon}}; \theta)$. The log-likelihood can be well decomposed,

$$\log \mathbf{p}(\tilde{\boldsymbol{\varepsilon}}) = \log \mathbf{p}(\mathbf{h}_\theta(\tilde{\boldsymbol{\varepsilon}})) + \sum_{i=1}^k \log \left| \det \frac{\partial \mathbf{h}_i(\tilde{\boldsymbol{\varepsilon}}; \theta)}{\partial \tilde{\boldsymbol{\varepsilon}}} \right|. \quad (11)$$

For the prediction results $\{\hat{\mathbf{X}}_t\}_{t=1}^{T-1}$ of RC, it can be regarded as single-step predictions of trajectory data $\{\mathbf{X}_t\}_{t=0}^{T-2}$. Since we assume that $\mathbf{p}(\tilde{\boldsymbol{\varepsilon}})$ does not change over time, we can obtain a total of $M \times (T - 1)$ samples of $\tilde{\boldsymbol{\varepsilon}}$. To learn the transformation \mathbf{h}_θ , we minimize the following negative log-likelihood,

$$\begin{aligned} \mathcal{L}_{NF} &= - \sum_{j=1}^{M(T-1)} \log \mathbf{p}(\tilde{\boldsymbol{\varepsilon}}^{(j)}) \\ &= - \sum_{j=1}^{M(T-1)} \left(\log \mathbf{p}(\mathbf{h}_\theta(\tilde{\boldsymbol{\varepsilon}}^{(j)})) + \sum_{i=1}^k \log \left| \det \frac{\partial \mathbf{h}_i(\tilde{\boldsymbol{\varepsilon}}^{(j)}; \theta)}{\partial \tilde{\boldsymbol{\varepsilon}}^{(j)}} \right| \right). \end{aligned} \quad (12)$$

That is, maximizing the log-likelihood function of $\tilde{\boldsymbol{\varepsilon}}$. After training, it is easy to sample from the target distribution as long as \mathbf{h}_θ^{-1} is tractable. It is only necessary to sample from the Gaussian distribution \mathbf{u} and apply \mathbf{h}_θ^{-1} to these samples. We note that the prediction $\tilde{\mathbf{X}}_t$ is the RC one-step prediction $\hat{\mathbf{X}}_t$ corrected by NF error distribution $\tilde{\boldsymbol{\varepsilon}}$, i.e., $\tilde{\mathbf{X}}_t = \hat{\mathbf{X}}_t + \tilde{\boldsymbol{\varepsilon}}$ for $t \geq T$. In this way, we are able to forecast the long-term evolution of stochastic process \mathbf{X} .

For the invertible and differentiable mapping \mathbf{h}_θ , general options include Real NVP, ActNorm, Masked Autoregressive Flow, and others [47]. The rational-quadratic neural splines flow which may feature autoregressive layers (RQ-NSF (AR)) [45] is used in this article. Rational Quadratic Splines (RQS) denote \mathbf{h}_θ as a monotone rational-quadratic spline on an interval as the identity function otherwise. The spline is defined by $K + 1$ knots and the derivatives at the $K - 1$ inner points. The positions of these knots and their corresponding derivatives are represented by the output of a neural network. An autoregressive layer is utilized to generate each entry of the output based on the previous entries of the input. We write RQ-NSF (AR) as:

$$h_\theta^i(\tilde{\boldsymbol{\varepsilon}}^i) = \text{RQS}_{\Theta(\tilde{\boldsymbol{\varepsilon}}^{1:i-1})}(\tilde{\boldsymbol{\varepsilon}}^i), \quad \text{for } i = 1, \dots, d, \quad (13)$$

where RQS represents the Rational Quadratic Splines method, Θ is a neural network.

3.3 Combining Reservoir Computing and Normalizing Flow

Reservoir computing is good at capturing the evolutionary trend of the system, making it suitable as a surrogate model for long-term system prediction. Unlike the prediction of a deterministic system, normalizing flows are introduced as a compensatory mechanism for error modeling due to the presence of inherent noise. In this section, we provide a framework for modeling and predicting stochastic dynamical systems by combining Reservoir Computing and Normalizing Flow. For the sake of convenience, we shall henceforth refer to this method as RC-NF.

- **Data:** We generate M trajectories with a total length of $T + T_{valid} + T_{test}$ from SDE (1) or SDDE (3). To train the model, we utilize the initial T states, validate it using the intermediate T_{valid} states, and test it using the final T_{test} states.

- **Training (Reservoir Computing):** Select a set of hyperparameters to generate matrices A , W_{in} and vector ζ to compose the reservoir structure. M trajectories entered the reservoir by matrix W_{in} in chronological order and obtained the reservoir state \mathbf{r}_t by formula (4). The first T_{warm} states are used to warm up the RC framework in order to eliminate the influence of the given initial value \mathbf{r}_0 . After the warm-up, trajectory data with a total length of time $T - T_{warm} - 1$ is used to train W_{out} through Tikhonov transformation (8). Utilizing the matrix W_{out} , one-step prediction $\hat{\mathbf{X}}_t$ is obtained by (6).

- **Validation (Reservoir Computing):** Based on the trained readout matrix W_{out} , roll predictions are made at a few T_{valid} steps. The \mathcal{L}_2 error between the forecast $\hat{\mathbf{X}}_t$ and the data \mathbf{X}_t , $\mathcal{L}_2 = \sum_{t=T+1}^{T+T_{valid}} (\hat{\mathbf{X}}_t - \mathbf{X}_t)^2$, is calculated as a loss function of Bayesian Optimization. BO refines the set of hyperparameters by utilizing the posterior distribution of the loss function, before resuming the training phase with the updated parameters. We select the set of hyperparameters that correspond to the minimum \mathcal{L}_2 loss during the BO iteration process as the optimal hyperparameters for RC.

- **Training (Normalizing Flow):** Based on the readout matrix W_{out} and single-step prediction $\hat{\mathbf{X}}_t$ obtained by the optimal RC hyperparameters, we collect $M \times (T - T_{warm} - 1)$ samples of the single-step error $\tilde{\varepsilon}$ during the training phase. Subsequently, Normalizing Flow is used to estimate the probability density function $\mathbf{p}(\tilde{\varepsilon})$ from these samples, obtaining the optimal mapping \mathbf{h}_θ between the target distribution and a pre-specified base distribution.

- **Testing (long-term prediction):** For the m -th trajectory, the compensated one-step prediction can be expressed as $\tilde{\mathbf{X}}_t^{(m)} := \hat{\mathbf{X}}_t^{(m)} + \tilde{\varepsilon}^{(m)}$ where $\tilde{\varepsilon}^{(m)}$ is a new sample generated by NF, $t \in [T + T_{valid} + 1, T + T_{valid} + T_{test}]$. Regarding $\tilde{\mathbf{X}}_t^{(m)}$ as the input of the RC framework at time $t + 1$, our strategy results in rolling long-term predictions for the m -th trajectory. If there are enough trajectories of the stochastic process \mathbf{X} , the probability density $\mathbf{p}(\mathbf{X}_t)$ of \mathbf{X} at time t can be approximated effectively.

- **Generating:** For the reservoir structure A , W_{in} , W_{out} and the probability density $\mathbf{p}(\tilde{\varepsilon})$ of error are learned by the fixed stochastic dynamical system, a trajectory of any length can be generated by rolling a short warm-up trajectory. More specifically, assume a short trajectory $\{\mathbf{X}_t\}_{t=0}^{T_{warm}-1}$ for warm-up, the input of RC at the time interval $[0, T_{warm} - 1]$ is given by this trajectory. After T_{warm} steps, the RC input is given by the corrected $\tilde{\mathbf{X}}_t$, which is obtained by plugging the compensated error of NF into the single-step prediction of RC.

Fig. 1(a) presents the overall framework in diagram form, while Fig. 1(b) depicts the time allocation for testing and generation tasks. Additionally, the pseudocode for RC-NF is outlined in Algorithm 1.

3.4 Universality of RC-NF

In this section, we will analyze the universality of RC-NF mentioned in Sec. 3.3. For d -dimensional SDEs (1) or SDDEs (3), assume the drift and diffusion coefficients satisfy the Lipschitz and growth conditions so that solutions of them exist and are unique [1, 3, 5].

- **Convergence of numerical scheme**

When dealing with real or simulation data, we can obtain trajectory data through discrete-time observations or through numerical simulations of SDE (1) or SDDE (3). Let $\{\mathbf{X}_t^{\delta t}\}$ be discrete-time observations or the numerical solution of SDE (1) or SDDE (3) with (maximal) time step size δt in this section. $\{\mathbf{X}_t^{\delta t}\}$ and $\{\mathbf{X}_t\}$ are not distinguished in the other sections.

The most commonly used numerical scheme for SDE (1) is the Euler-Maruyama scheme:

$$\mathbf{X}_{t+\delta t} = \mathbf{X}_t + \mathbf{f}(\mathbf{X}_t)\delta t + \mathbf{g}(\mathbf{X}_t)\delta \mathbf{B}_t, \quad (14)$$

where $\delta \mathbf{B}_t \sim N(\mathbf{0}, \delta t \mathbf{I})$. Then the Euler-Maruyama scheme has the following convergence result.

Lemma 1. (Weinan E [5], Proposition 7.22) *The Euler-Maruyama scheme is of strong order 1/2. More specifically,*

$$\max_{0 \leq t \leq T} \mathbb{E} |\mathbf{X}_t^{\delta t} - \mathbf{X}_t|^2 \leq C(\delta t), \quad (15)$$

where C is a constant independent of δt .

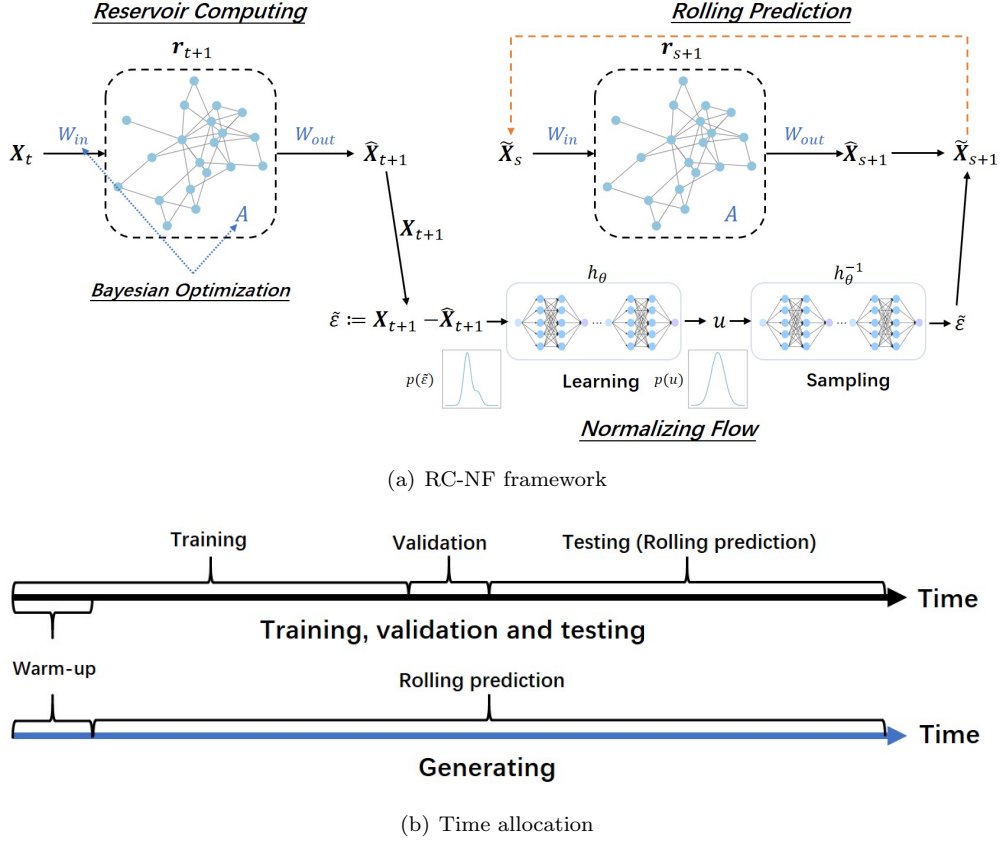


Figure 1: (a) The flowchart of RC-NF. In the training phase, the RC readout matrix W_{out} is trained according to multiple trajectory data and Tikhonov transformation, and the hyperparameters of RC fixed structure are searched by BO. NF is used to learn the probability density of the single-step prediction error $\tilde{\epsilon}$. Rolling predictions \tilde{X}_s are obtained by plugging the compensated error $\tilde{\epsilon}$ into the RC single-step prediction \tilde{X}_s . (b) Time allocation for tasks of testing and generating new trajectories. Both require a short warm-up phase.

The numerical scheme and convergence of SDDEs (3) can be found in [3]. These convergence results mean that as the time step $\delta t \rightarrow 0$, the numerical solutions converge to the corresponding solutions of SDE (1) or SDDE (3).

• Universality of Reservoir Computing

We introduce some notations and background knowledge on filters and reservoir systems, from discrete-time setup. For more details, see [36, 37, 53]. Let $\mathbb{Z} = \{\dots, -1, 0, 1, \dots\}$ and $\mathbb{Z}_- = \{\dots, -1, 0\}$. The sets $(\mathbb{R}^d)^{\mathbb{Z}}$ and $(\mathbb{R}^d)^{\mathbb{Z}_-}$ are composed of infinite \mathbb{R}^d -valued sequences of the type $(\dots, z_{-1}, z_0, z_1, \dots)$ and (\dots, z_{-1}, z_0) . Denote the space of real $n \times m$ matrices by $\mathbb{M}_{n,m}$, \mathbb{M}_n for the space of n -dimensional square matrices.

A filter is a map $U : (\mathbb{R}^d)^{\mathbb{Z}} \rightarrow \mathbb{R}^{\mathbb{Z}}$. If for any $z, z' \in (\mathbb{R}^d)^{\mathbb{Z}}$ which satisfy $z_s = z'_s$ for all $s \leq t$ for a given $t \in \mathbb{Z}$, one has that $U(z)_t = U(z')_t$, then the filter U is called **causal**. Define the time delay operator $T_{-s} : (\mathbb{R}^d)^{\mathbb{Z}} \rightarrow (\mathbb{R}^d)^{\mathbb{Z}}$ by $T_{-s}(z)_t := z_{t+s}$ for any $s \in \mathbb{Z}$. A **time-invariant** filter U refers that for all $s \in \mathbb{Z}$, $T_{-s} \circ U = U \circ T_{-s}$.

We refer to a map $H : (\mathbb{R}^d)^{\mathbb{Z}_-} \rightarrow \mathbb{R}$ as a functional. Causal and time-invariant filters can be equivalently described through the use of their naturally associated functionals. Given a causal and time-invariant U , its associated functional is defined by $H_U(z) := U(z^e)_0$, where z^e is an arbitrary extension of $z \in (\mathbb{R}^d)^{\mathbb{Z}_-}$ to $(\mathbb{R}^d)^{\mathbb{Z}}$. Conversely, one may define a causal and time-invariant filter $U_H : (\mathbb{R}^d)^{\mathbb{Z}} \rightarrow \mathbb{R}^{\mathbb{Z}}$ through a given functional H by setting $U_H(z)_t := H(\pi_{\mathbb{Z}_-} \circ T_{-t}(z))$ where $z \in (\mathbb{R}^d)^{\mathbb{Z}}$, $\pi_{\mathbb{Z}_-} : (\mathbb{R}^d)^{\mathbb{Z}} \rightarrow (\mathbb{R}^d)^{\mathbb{Z}_-}$ is the natural projection. The above maps U , T_s , H , and $\pi_{\mathbb{Z}_-}$ can be naturally extended to the measure space $((\mathbb{R}^d)^{\mathbb{Z}}, \otimes_{t \in \mathbb{Z}} \mathcal{B}(\mathbb{R}^d))$ (a general notation with no specific correspondence). We use the capital bold letter \mathbf{Z} to indicate a sequence of a d -dimensional discrete

Algorithm 1: Reservoir Computing with Normalizing Flow

Input: trajectories $\mathbf{X}_t^{(m)}$, $m = 1, \dots, M$, $t = 0, \dots, T - 1$;
Output: RC readout matrix W_{out} , probability density of the single-step error $\mathbf{p}(\tilde{\boldsymbol{\varepsilon}})$;
Initialization:
 hyperparameters selected by BO: the spectral radius ρ and average degree $\langle k \rangle$ of adjacency matrix A , the sampling range χ of elements of W_{in} , leakage factor α , regularization parameter λ ;
 random variable $u \sim N(\mathbf{0}, \mathbf{I})$;
Construct: ▷ Reservoir Computing
 matrices A , W_{in} , vector $\boldsymbol{\zeta}$;
for $m = 1 : M$ **do**
 for $t = 1 : T - 1$ **do**
 calculate and record reservoir states $\mathbf{r}_t^{(m)}$;
 end
end
Construct:
 states matrix $\mathbf{R} = [\dots, [1; \mathbf{X}_{t-1}^{(m)}; \mathbf{r}_t^{(m)}]^T, \dots]$, $m = 1, \dots, M$, $t = 1, \dots, T - 1$;
 observation matrix $\mathbf{Y} = [\dots, \mathbf{X}_t^{(m)}, \dots]$, $m = 1, \dots, M$, $t = 1, \dots, T - 1$;
 readout matrix $W_{out} = \mathbf{Y}\mathbf{R}^T(\mathbf{R}\mathbf{R}^T + \lambda\mathbf{I})^{-1}$;
for $m = 1 : M$ **do** ▷ Collection of single-step error samples
 for $t = 1 : T - 1$ **do**
 calculate the one-step prediction $\hat{\mathbf{X}}_t^{(m)} = W_{out}[1; \mathbf{X}_{t-1}^{(m)}; \mathbf{r}_t^{(m)}]^T$;
 calculate the one-step error sample $\tilde{\boldsymbol{\varepsilon}}_t^{(m)} = \hat{\mathbf{X}}_t^{(m)} - \mathbf{X}_t^{(m)}$;
 end
end
while $i \leq \textit{iterations}$ **do** ▷ Normalizing Flow
 calculate the loss function \mathcal{L}_{NF} ;
 update the parameters of function \mathbf{h}_θ ;
end
Obtain:
 probability density of the single-step error $\mathbf{p}(\tilde{\boldsymbol{\varepsilon}}) = \mathbf{p}(\mathbf{h}_\theta^{-1}(\mathbf{u}))$;
Result: Single-step prediction $\tilde{\mathbf{X}}_s^{(m)} := \hat{\mathbf{X}}_s^{(m)} + \tilde{\boldsymbol{\varepsilon}}^{(m)}$ for $s \geq T$, where the sample $\tilde{\boldsymbol{\varepsilon}}^{(m)}$ is sampled from the probability density function $\mathbf{p}(\tilde{\boldsymbol{\varepsilon}})$.

stochastic process.

The echo state network (ESN) [21] can be formulated as:

$$\begin{cases} \mathbf{r}_t = \sigma(A\mathbf{r}_{t-1} + W_{in}\mathbf{z}_t + \boldsymbol{\zeta}), \\ y_t = \mathbf{w}^T \mathbf{r}_t, \end{cases} \quad (16)$$

where $(\mathbf{z}_t)_{t \in \mathbb{Z}}$, $(y_t)_{t \in \mathbb{Z}}$ represent d -dimensional input and one-dimensional output discrete time sequences respectively. The symbol A , W_{in} , $\boldsymbol{\zeta}$, \mathbf{r}_t are consistent with definitions in Sec. 3.1. The map $\sigma : \mathbb{R} \rightarrow \mathbb{R}$ is an activation function that is applied element-wise to the vector. The vector \mathbf{w} is a readout matrix. A filter obtained by ESN (16) satisfies the so-called echo state property (ESP) given by the following statement [35, 36]: for any $\mathbf{z} \in (\mathbb{R}^d)^{\mathbb{Z}}$, there exists a unique $\mathbf{r} \in (\mathbb{R}^N)^{\mathbb{Z}}$ such that the first formula of (16) holds.

Remark 1. *There are slight differences between the ESN and RC mentioned in Sec. 3.1. Actually, the \mathbf{r}_t update rule (4) contains one more item $(1 - \alpha)\mathbf{r}_t$ that explicitly correlates \mathbf{r}_t and \mathbf{r}_{t+1} to represent memory and use α to control the amplitude. Additionally, the additional $1+d$ dimensions of the row of W_{out} (8) are used to explicitly correlate inputs and outputs as well as to include a bias term. These are all to enhance the robustness of the model when used in practice. Appendix A.1 explores an experiment on how ESN and RC differed, and the RC results are marginally superior.*

Based on the theorem in [36] (Lemma A1 in Appendix A), we show that if the time delay operator is bounded, then filters of the form (16) are identical in the L^p -sense when the input sequences can be represented by each other using time delay operators.

Theorem 1. *Let U be a causal and time-invariant filter and its associated functional is H . Fix $p \in [1, \infty)$, let \mathbf{Z} be a fixed \mathbb{R}^d -valued input process, and $H(\pi_{\mathbb{Z}_-}(\mathbf{Z})) \in L^p(\Omega, \mathcal{F}, \mathbb{P})$. Assume the time delay operator T_{-s} is a bounded operator for any $s \in \mathbb{Z}$. Then there exists causal and time-invariant filters U' , $U^{s'}$ satisfying (16), constructed by input sequences $\pi_{\mathbb{Z}_-}(\mathbf{Z})$, $\pi_{\mathbb{Z}_-} \circ T_{-s}(\mathbf{Z})$, respectively, that are identical in the L^p -sense. That is, $\|U'(\mathbf{Z})_s - U^{s'}(\mathbf{Z})_s\|_p < (\|T_{-s}\|_p + 1)\varepsilon$.*

The proof of this theorem is shown in Appendix A.

For the d -dimensional stochastic process $(\mathbf{X}_t)_{t \in [0, T]}$ defined by SDE (1) or SDDE (3), $\mathbf{X}_t \in L^2(\Omega, \mathcal{F}, \mathbb{P})$ can be satisfied by the Lipschitz and growth conditions of the drift and diffusion coefficients. We can construct countable infinite discrete sequences with respect to the process \mathbf{X} for $t \in [0, T]$, denote as $(\mathbf{X}_t)_{t \in \mathbb{Z}} := (\dots, \mathbf{X}_{t-1}, \mathbf{X}_t, \mathbf{X}_{t+1}, \dots)$. The counterpart based on the Euler-Maruyama scheme is denoted as $(\mathbf{X}_t^{\delta t})_{t \in \mathbb{Z}} := (\dots, \mathbf{X}_{t-1}^{\delta t}, \mathbf{X}_t^{\delta t}, \mathbf{X}_{t+1}^{\delta t}, \dots)$. Due to Lemma 1, $\mathbf{X}_t^{\delta t} \in L^2(\Omega, \mathcal{F}, \mathbb{P})$ for all $t \in \mathbb{Z}$. We generalize the conclusions of Lemma A1 and Theorem 1 to discrete time series $(\mathbf{X}_t^{\delta t})_{t \in \mathbb{Z}}$ based on the numerical scheme.

Theorem 2. *Define a filter $U : ((\mathbb{R}^d)^{\mathbb{Z}}, \otimes_{t \in \mathbb{Z}} \mathcal{B}(\mathbb{R}^d)) \rightarrow ((\mathbb{R}^d)^{\mathbb{Z}}, \otimes_{t \in \mathbb{Z}} \mathcal{B}(\mathbb{R}^d))$ by $U((\mathbf{X}_t^{\delta t})_{t \in \mathbb{Z}})_t = \mathbf{X}_{t+1}^{\delta t}$. Let $(\mathbf{X}_t^{\delta t})^{(1)} := (\dots, \mathbf{X}_{t-1}^{\delta t}, \mathbf{X}_t^{\delta t})$ be a fixed \mathbb{R}^d -valued input process. Then for arbitrary $\varepsilon > 0$, there exists $N \in \mathbb{N}$, $W_{in} \in \mathbb{M}_{N, d}$, $\zeta \in \mathbb{R}^d$, $A \in \mathbb{M}_N$, $\mathbf{w} \in \mathbb{R}^N$ such that (16) has the ESP, the corresponding filter is causal and time-invariant, the associated functional satisfies $\mathbf{H}_{\mathbf{w}}^{A, W_{in}, \zeta}((\mathbf{X}_t^{\delta t})^{(1)}) \in L^2(\Omega, \mathcal{F}, \mathbb{P})$ and*

$$\|\mathbf{H}((\mathbf{X}_t^{\delta t})^{(1)}) - \mathbf{H}_{\mathbf{w}}^{A, W_{in}, \zeta}((\mathbf{X}_t^{\delta t})^{(1)})\|_2 < \varepsilon. \quad (17)$$

Additionally, for any $s \in \mathbb{Z}$, consider input sequences $(\mathbf{X}_t^{\delta t})^{(1)}$ and $T_{-s}((\mathbf{X}_t^{\delta t})^{(1)})$, there exists causal and time-invariant filters U' , $U^{s'}$ satisfying (16), constructed by input sequences $(\mathbf{X}_t^{\delta t})^{(1)}$, $T_{-s}((\mathbf{X}_t^{\delta t})^{(1)})$, that are identical in the L^2 -sense.

Appendix A provides the proof for this theorem.

Remark 2. *As revealed in Theorem 1 and Theorem 2, for arbitrary $\varepsilon > 0$, we have $\|U'((\mathbf{X}_t^{\delta t})_{t \in \mathbb{Z}})_s - U^{s'}((\mathbf{X}_t^{\delta t})_{t \in \mathbb{Z}})_s\|_2 < \varepsilon$ for arbitrary $s \in \mathbb{Z}$, where U' and $U^{s'}$ are filters of the form (16) constructed by Lemma A1 and the corresponding input sequences can be represented by time delay operators to each other. We use the notation $\hat{\mathbf{X}}_t$ in Sec. 3.1 to indicate the output of ESN. The above conclusion means that for a semi-infinite input sequence of the form $(\mathbf{X}_t^{\delta t})^{(1)}$, $\|\hat{\mathbf{X}}_{t+1} - \mathbf{X}_{t+1}^{\delta t}\|_2 = \|U'((\mathbf{X}_t^{\delta t})^{(1)})_0 - U((\mathbf{X}_t^{\delta t})^{(1)})_0\|_2 = \|\mathbf{H}'((\mathbf{X}_t^{\delta t})^{(1)}) - \mathbf{H}((\mathbf{X}_t^{\delta t})^{(1)})\|_2 < \varepsilon$, for all $t \in \mathbb{Z}$. Furthermore, this shows that a filter of the form (16) can approximate the numerical solution $\{\mathbf{X}_t^{\delta t}\}$ in the L^2 -sense, which is denoted as $\{\hat{\mathbf{X}}_t\}$. Lemma 1 states that the numerical solution $\{\mathbf{X}_t^{\delta t}\}$ converges to solutions of SDEs (1) or SDDEs (3) when the time step $\delta t \rightarrow 0$. The current theoretical results are derived from discrete time series, and further investigation is required to determine whether the theorems in this section hold for continuous-time stochastic processes in the time domain of $[0, T]$.*

• Universality of Normalizing Flow

According to Theorem 1 and Theorem 2, given sufficient data, RC can serve as a universal approximator for the stochastic dynamical systems under study. It is worth noting that during the testing phase (prediction phase), there is no data available to provide us with information about the system. Therefore, there are significant differences between the training and testing phases. Each step of the training phase input $\mathbf{X}_t^{\delta t}$ is from SDE (1) or SDDE (3), with information both on drift and diffusion coefficients. In the testing phase, revisit formulas (4), (6) for RC or (16) for ESN, with the input $\mathbf{X}_t^{\delta t}$ replaced by the predicted output $\hat{\mathbf{X}}_t$ of the preceding step, the evolution laws of reservoir states \mathbf{r}_t are polluted by prediction errors. Rolling predictions, on the other hand, necessarily lead to a rapid accumulation of errors. According to these justifications, the RC model fails as the discrepancy between the stochastic process predicted by RC and the target stochastic process widens with increasing prediction time.

If we can guarantee that the input stochastic process remains fixed during the testing phase, RC is still a reasonable approximator. More specifically, our objective is to accurately predict the state $\mathbf{X}_{T+k}^{\delta t}$ in the sense of probability distribution, where $k > 0$ is an integer, that is, the goal is to estimate

the probability density $\mathbf{p}(\mathbf{X}_{T+k}^{\delta t})$ from data. Therefore, the task of NF introduced in Sec. 3.2 is to correct the probability density of output $\hat{\mathbf{X}}_{T+1}$ to $\mathbf{p}(\mathbf{X}_{T+1}^{\delta t} | \mathbf{X}_T^{\delta t} = \mathbf{x})$ in single-step prediction, that is, $\mathbf{p}(\mathbf{X}_{T+1}^{\delta t}) = \int_{\mathbb{R}^d} \mathbf{p}(\mathbf{X}_{T+1}^{\delta t} | \mathbf{X}_T^{\delta t} = \mathbf{x}) \mathbf{p}_{\mathbf{X}_T^{\delta t}}(d\mathbf{x})$.

It should be noticed that the diffusion coefficient matrix \mathbf{g} is a constant diagonal matrix, namely, the SDE/SDDE with additive noise. Besides, based on the observation of numerical experiments presented in Sec. 4, we propose the following assumption. Further exploration of this issue is left for future research.

Assumption 1. *If we fix the time interval δt between $\mathbf{X}_{t+1}^{\delta t}$ and $\mathbf{X}_t^{\delta t}$ for all $t \in \mathbb{Z}$, then the single-step prediction error $\tilde{\varepsilon} := \mathbf{X}_{t+1}^{\delta t} - \hat{\mathbf{X}}_{t+1}$ between the true filter U and the filter U' of the form (16) obtained by Theorem 2 has the same distribution at each time t , that is, $\mathbf{p}(\tilde{\varepsilon})$ is fixed for all $t \in \mathbb{Z}$.*

Assumption 1 implies that $\tilde{\varepsilon}$ is independent of single-step prediction $\hat{\mathbf{X}}_{t+1}$. For a special class of transformation \mathbf{h}_θ (9), we can conclude the following universality with respect to NF.

A mapping $\mathbf{h}_\theta = (h_\theta^{(1)}, \dots, h_\theta^{(d)}) : \mathbb{R}^d \rightarrow \mathbb{R}^d$ is called **triangular** if h_θ^i is a function of $\mathbf{u}^{1:i}$ for each $i = 1, \dots, d$, where $\mathbf{u} = (u^1, \dots, u^d) \in \mathbb{R}^d$. Such a triangular map \mathbf{h}_θ is called **increasing** if h_θ^i is an increasing function of u^i for each i .

Proposition 1. *(Kobzyev [47], Proposition 4) If μ and ν are absolutely continuous Borel probability measures on \mathbb{R}^d , then there exists an increasing triangular transformation $\mathbf{h}_\theta : \mathbb{R}^d \rightarrow \mathbb{R}^d$, such that $\nu = \mathbf{h}_{\theta*}\mu$. This transformation is unique up to null sets of μ . A similar result holds for measures on $[0, 1]^d$.*

Proposition 2. *(Kobzyev [47], Proposition 5) If μ is an absolutely continuous Borel probability measure on \mathbb{R}^d and $\{\mathbf{h}_{\theta_n}\}$ is a sequence of maps $\mathbb{R}^d \rightarrow \mathbb{R}^d$ which converges pointwise to a map \mathbf{h}_θ , then a sequence of measures $(\mathbf{h}_{\theta_n})_*\mu$ weakly converges to $\mathbf{h}_{\theta*}\mu$.*

Using Proposition 1 and Proposition 2, universality could be proved for spline flows [45] with splines for coupling functions. In fact, RQ-NSF (AR) (in Sec. 3.2) itself is a triangular and increasing map. The iterative training of NF is to construct a sequence of maps $\{\mathbf{h}_{\theta_n}\}$, for $n = 1, 2, \dots$, to approximate the required transformation \mathbf{h}_θ , and the result follows. For more specific explanations, we recommend [45, 54].

So far, we show that NF with specific transformation \mathbf{h}_θ (RQ-NSF (AR)) can approximate the probability measure $\mu_{\tilde{\varepsilon}}$ or the probability density function $\mathbf{p}(\tilde{\varepsilon})$. Following a single-step error correction, the conditional probability density function $\mathbf{p}(\hat{\mathbf{X}}_{T+1} + \tilde{\varepsilon} | \mathbf{X}_T^{\delta t} = \mathbf{x})$ is identical to the true conditional probability density function $\mathbf{p}(\mathbf{X}_{T+1}^{\delta t} | \mathbf{X}_T^{\delta t} = \mathbf{x})$. Furthermore, a simple derivation, $\mathbf{p}(\hat{\mathbf{X}}_{T+1} + \tilde{\varepsilon}) = \int_{\mathbb{R}^d} \mathbf{p}(\hat{\mathbf{X}}_{T+1} + \tilde{\varepsilon} | \mathbf{X}_T^{\delta t} = \mathbf{x}) \mathbf{p}_{\mathbf{X}_T^{\delta t}}(d\mathbf{x}) = \int_{\mathbb{R}^d} \mathbf{p}(\mathbf{X}_{T+1}^{\delta t} | \mathbf{X}_T^{\delta t} = \mathbf{x}) \mathbf{p}_{\mathbf{X}_T^{\delta t}}(d\mathbf{x}) = \mathbf{p}(\mathbf{X}_{T+1}^{\delta t})$, yields the desired result, that is, $\hat{\mathbf{X}}_{T+1} + \tilde{\varepsilon}$ and $\mathbf{X}_{T+1}^{\delta t}$ have the same distribution. We follow the notation $\tilde{\mathbf{X}}_{T+1} := \hat{\mathbf{X}}_{T+1} + \tilde{\varepsilon}$ in Sec. 3.2 to represent the RC prediction $\hat{\mathbf{X}}_{T+1}$ corrected by the NF single-step error modeling $\tilde{\varepsilon}$. The prediction $\tilde{\mathbf{X}}_{T+1}$ is used as the next step input of RC and the RC output result is corrected by NF error distribution again. Repeating this step, we can utilize RC-NF to achieve long-term predictions of stochastic dynamical systems.

4 Experiments

This section aims to demonstrate the effectiveness of our method, RC-NF, by exploring it from multiple angles. To be specific, our analysis takes into account the effects of linear/non-linear systems, Markov/non-Markov processes, stationary/non-stationary models, and a chaotic system on RC-NF. We summarize a list of experiments as follows.

- The Ornstein-Uhlenbeck process (OU process) is a simple linear system, which serves as the first example we validate.
- The Double-well system (DW system) exhibits transition phenomena, and we can not only make long-term predictions but also accurately capture its transition rates.
- We employ a linear SDDE to illustrate the impact of the RC-NF framework on non-Markovian stochastic systems with time delays.

- The El Niño Southern Oscillation (ENSO) simplified model is a complex time-delay system that is non-linear, non-Markovian, and non-stationary. Moreover, it demonstrates the remarkable ability of RC-NF.
- The stochastic Lorenz system, a chaotic system, is employed to demonstrate the substantial improvement of RC-NF over RC through the evaluation of multiple criteria (probability density function, maximum Lyapunov exponent, close returns, autocorrelation function, and cross-correlation function).

We use the Euler-Maruyama scheme to generate trajectory data for all experiments. For all systems, with the exception of the stochastic Lorenz system, we assume that the numerical scheme step size δt and the observation time step (or sampling time step) Δt are equal. We choose 500 reservoir nodes for one-dimensional systems and 1000 reservoir nodes for the three-dimensional system. The hyperparameters of RC chosen by BO for various experiments are displayed in Appendix B.

We utilize RQ-NSF(AR) as the foundational transformation for normalizing flow and apply it twice through composition to obtain the final transformation \mathbf{h}_θ (9). Our base neural network consists of a fully connected neural network with two hidden layers, each containing 8 nodes. To train the model, we use the Adam optimizer with a learning rate of 0.005 and perform 500 iterations.

We list the common partial criteria across all experiments, along with their respective results in each experiment. The criteria for specific systems will be described in detail as needed. The Wasserstein distance is a distance function that measures the dissimilarity between probability distributions on a specific metric space. In the following, the Wasserstein 2-distance (W_2) is employed. The Kullback-Leibler divergence (KL divergence) is a measure of how one probability distribution P differs from a second, reference probability distribution Q , denoted as $D_{KL}(P\|Q)$. We employ them to measure the discrepancy between the probability distributions of the data and the forecasts generated by our surrogate model, RC-NF. Tables 2 and 3 show the Wasserstein distances $W_2(\mathbf{X}_t, \tilde{\mathbf{X}}_t)$ and KL divergences $D_{KL}(\tilde{\mathbf{X}}_t\|\mathbf{X}_t)$ at a number of predicted snapshots and the means of them across all predicted time.

Table 2: Wasserstein distances at a number of predicted snapshots and the means of Wasserstein distances across all predicted snapshots. Time t_i , $i = 1, \dots, 5$ represent the different forecasting snapshots we select. Each of these times 10^{-3} .

Experiments	t_1	t_2	t_3	t_4	t_5	Mean
OU process	10.494	11.959	13.173	14.349	17.374	12.385
DW system	5.3359	5.4639	5.4390	5.1680	5.1745	5.4179
Linear SDDE	8.9689	7.9715	8.6401	7.1655	7.9070	7.9967
ENSO simplified model	7.8604	5.7932	6.4838	7.9760	6.1406	6.4873

Table 3: KL divergences at a number of predicted snapshots and the means of KL divergences across all predicted snapshots. Time t_i , $i = 1, \dots, 5$ represent the different forecasting snapshots we select. Each of these times 10^{-3} .

Experiments	t_1	t_2	t_3	t_4	t_5	Mean
OU process	2.3487	2.2405	5.2048	3.4695	4.1003	2.6387
DW system	2.9123	4.9392	3.5568	0.9387	3.1716	3.1879
Linear SDDE	1.4285	1.6431	1.7739	2.0469	3.0536	1.7927
ENSO simplified model	3.9270	1.5115	7.4493	3.5715	2.2184	2.8313

4.1 Ornstein-Uhlenbeck process: long-term prediction

We describe the Ornstein-Uhlenbeck process (OU process) [1] as follows:

$$dX_t = b_0(\mu_0 - X_t)dt + gdB_t, \quad \text{for } t \geq 0, \quad (18)$$

where $b_0 > 0$ indicates the rate of mean reversion, $\mu_0 \in \mathbb{R}$ is the mean value, and the constant $g > 0$ is the volatility. B_t is a scalar Brownian motion. For a given initial state $X_0 = x$, the analytical

solution of the OU process is $X_t = (1 - e^{-b_0 t})\mu_0 + xe^{-b_0 t} + g \int_0^t e^{-b_0(t-s)} dB_s$. More specifically, $X_t \sim N(\mu_0 + (x - \mu_0)e^{-b_0 t}, g^2 \int_0^t e^{-2b_0(t-s)} ds)$. The solution X_t is a stationary process that admits a Gaussian distribution $N(\mu_0, g^2/2b_0)$ when $t \rightarrow \infty$.

Assuming that the parameters of the system are $b_0 = 0.15$, $\mu_0 = 1$, and $g = 1$. We use the Euler-Maruyama scheme for solving this system with time step $\delta t = 0.01$, and the observed data are recorded at every time step, i.e., $\Delta t = 0.01$. The initial value is $X_0 = 0$. We generate 1000 trajectories with a total length of 4000, where the training length T , verification length T_{valid} , and prediction length T_{test} are 2000, 100, and 1900 respectively, and the first 100 steps of training are used for warm-up.

First, Fig. 2 shows the significant difference between RC and RC-NF in their ability to predict the OU process. Since the OU process follows Gaussian distribution at arbitrary fixed time t , we can build confidence intervals using the "three-sigma rule," which correspond to 68%, 95%, and 99.7% confidence intervals, respectively (magenta dashed lines in Fig. 2, the middle line represents the mean $\mu_0 + (x - \mu_0)e^{-b_0 t}$). The solid blue line denotes the sample mean, and the shaded blue portions from dark to light represent the intervals calculated from the trajectory data, which are made up of 68%, 95%, and 99.7% of the data surrounding the median at that moment. Rolling predictions using RC and RC-NF produce the red dotted dashes and shaded areas. The superior performance of RC-NF is demonstrated for the OU process. In fact, while RC alone is unable to provide an accurate forecast of the OU process distribution in the long run, the RC-NF framework is capable of doing so.

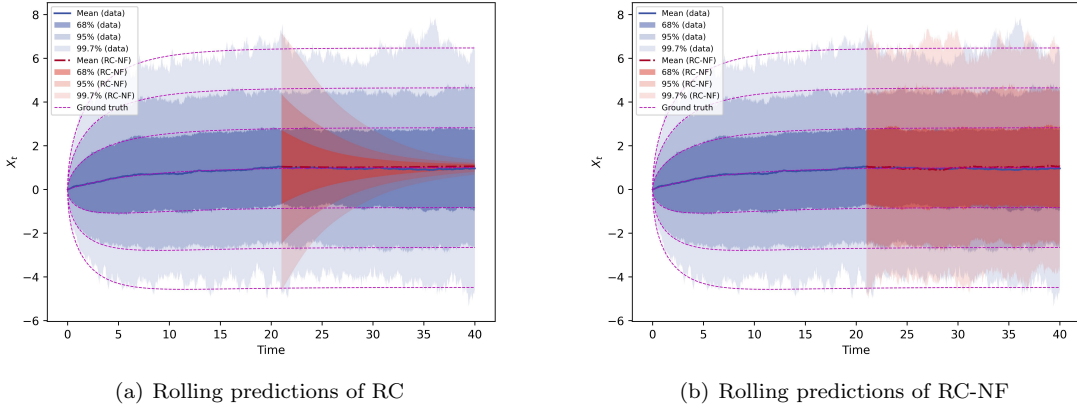


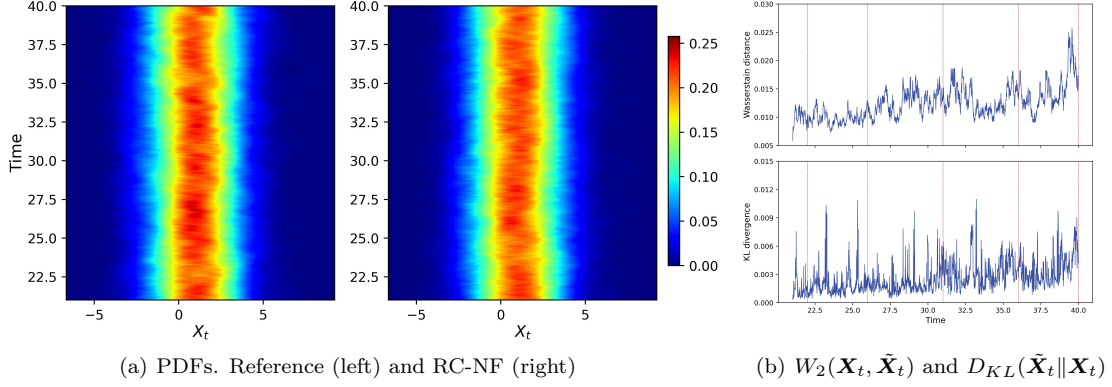
Figure 2: Rolling predictions of RC and RC-NF. The magenta dashed lines represent the theoretical true values of the mean and confidence intervals. The solid blue line denotes the sample mean, and the shaded blue portions from dark to light represent the intervals calculated from the trajectory data. Rolling predictions using RC and RC-NF produce the red dotted dashes and shaded areas. (a) Rolling predictions of RC; (b) Rolling predictions of RC-NF.

To further confirm the effectiveness of the RC-NF, Fig. 3(a) depicts the probability density functions of the trajectory data and the rolling predictions of RC-NF on the test dataset. Fig. 3(b) displays Wasserstein distances and KL divergences at different times on the test dataset; the red dashed lines represent the selected snapshots, and their probability density functions and specific values are displayed in Fig. 3(c) and Tables 2 and 3, respectively. The quantity of trajectory data is also a factor in the discrepancy between RC-NF predictions and trajectory data. Despite all of this, our proposed RC-NF has shown to be effective in achieving long-term prediction of the OU process, as demonstrated by these results. Even though the OU process is a linear, Markov, stationary process, traditional RC fails, and the success of RC-NF further makes us wonder how RC-NF will behave on more complex systems.

4.2 Double-Well system: transition rate

We consider a Double-Well system (DW system) [1, 17, 19] defined on \mathbb{R} ,

$$dX_t = (X_t - X_t^3)dt + g dB_t, \quad \text{for } t \geq 0, \quad (19)$$



(a) PDFs. Reference (left) and RC-NF (right) (b) $W_2(\mathbf{X}_t, \tilde{\mathbf{X}}_t)$ and $D_{KL}(\tilde{\mathbf{X}}_t \parallel \mathbf{X}_t)$

(c) PDFs. References (solid blue lines) and RC-NF results (red dashed lines) for several snapshots selected on the test dataset

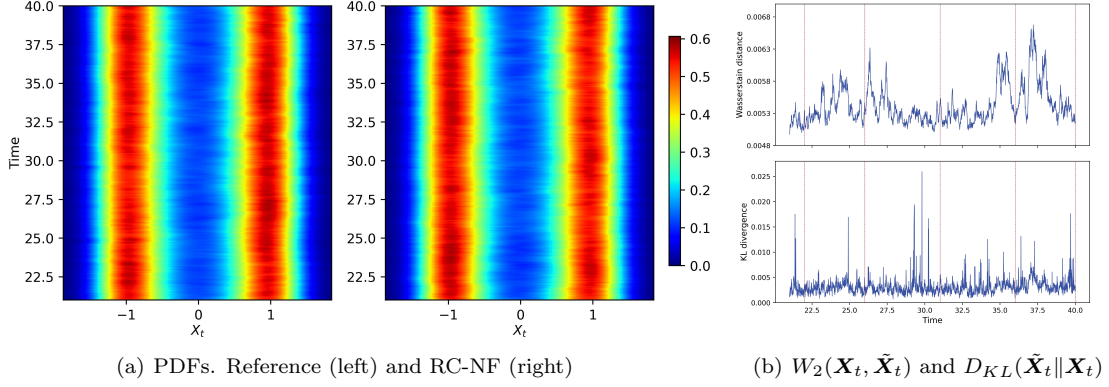
Figure 3: Results of the OU process. PDF is the abbreviation for probability density function. PDFs of the trajectory data and the RC-NF rolling predictions are shown in (a). (b) Wasserstein distance (top) and KL divergence (bottom), the red dashed lines represent snapshots where we draw the PDFs in (c) and display the values in Tables 2 and 3.

where the constant g is a positive diffusion coefficient and B_t is a scalar Brownian motion. This is a bistable system with its determined counterpart having two stable fixed points ($X_t = -1$, $X_t = 1$) and one unstable fixed point ($X_t = 0$). The trajectory from this system transitions between two metastable states under the influence of noise, which is not possible in the absence of noise.

Assume that $g = 0.5$ (larger noise makes it difficult to calculate the subsequent transition rate). We use the same time step size for this system as we do for the OU process, that is, $\delta t = \Delta t = 0.01$. The initial values X_0 are drawn from a uniform distribution on $[-1.5, 1.5]$. We generate 2000 trajectories with a total length of 4000 using the Euler-Maruyama scheme, where the training length T , verification length T_{valid} , and prediction length T_{test} are 2000, 100, and 1900 respectively, and the first 100 steps of training are used for warm-up.

Fig. 4(a) depicts the probability density functions of the trajectory data and the rolling predictions of RC-NF on the test dataset. Rolling predictions of RC-NF reproduce the bimodal probability density function of the DW system. The two peaks correspond to two metastabilities of the system. Fig. 4(b) displays Wasserstein distances and KL divergences at each time t in the testing phase; the red dashed lines represent the selected snapshots, and their probability density functions and specific values are displayed in Fig. 4(c) and Tables 2 and 3, respectively. The results demonstrate the efficiency of our proposed RC-NF framework and its remarkable ability to predict the DW system over the long term.

The transition phenomenon of trajectories between two metastabilities in the DW system is a rare event, and it is also known as noise-induced tipping [7]. We use the trained RC-NF model to generate new sample trajectories based on a small number of data to verify whether it can approximate the transition rate of the rare event. Following [19, 55], we first separate the phase space for X_t into $A = (-\infty, 0]$ and $B = (0, +\infty)$ regions in order to calculate the transition rate between the two states.



(a) PDFs. Reference (left) and RC-NF (right) (b) $W_2(\mathbf{X}_t, \tilde{\mathbf{X}}_t)$ and $D_{KL}(\tilde{\mathbf{X}}_t \parallel \mathbf{X}_t)$

(c) PDFs. References (solid blue lines) and RC-NF results (red dashed lines) for several snapshots selected on the test dataset

Figure 4: Results of the DW system. PDFs of the trajectory data and the RC-NF rolling predictions are shown in (a). (b) Wasserstein distance (top) and KL divergence (bottom), the red dashed lines represent snapshots where we draw the PDFs in (c) and display the values in Tables 2 and 3.

The time correlation function $C_{AB}(t)$ is defined as follows:

$$\frac{C_{AB}(t)}{C_A} = \frac{\langle I_A(X_0)I_B(X_t) \rangle}{\langle I_A(X_0) \rangle}, \quad (20)$$

where $I_A(\cdot)$ is an indicator function satisfying $I_A(X_t) = 1$ if $X_t \in A$, and $I_A(X_t) = 0$ if $X_t \notin A$, and $I_B(X_t)$ is defined similarly. The symbol $\langle \cdot \rangle$ denotes the ensemble average. When the system is originally in the region A , the ratio (20) represents the probability of discovering it in the region B after time t . The ratio C_{BA} can be analogously defined. Furthermore, the transition rate from A to B can be calculated as:

$$k_{AB} = \frac{d}{dt} \frac{C_{AB}(t)}{C_A}, \quad \text{for } \tau_{mol} < t \ll \tau_{rxn}, \quad (21)$$

where τ_{mol} is a short transient time [55] and $\tau_{rxn} = 1/(k_{AB} + k_{BA})$ is the exponential relaxation time. k_{AB} is actually the slope of the time correlation function $C_{AB}(t)$ for $\tau_{mol} < t \ll \tau_{rxn}$. For the calculation of transition rate k_{AB} , we set the initial value $X_0 = -1$. A small piece of data of length $T_{warm} = 100$ is used to warm up, and 2000 trajectories are generated by the Euler-Maruyama scheme and the trained RC-NF model, respectively. Utilizing equations (20) and (21), the transition rates of trajectory data (denoted as k_{AB}) and of generating trajectories by the RC-NF model (denoted as \tilde{k}_{AB}) can be calculated. The transition rate k_{BA} is calculated similarly, except that the initial value $X_0 = 1$. Fig. 5 shows the calculated results of C_{AB}/C_A and C_{BA}/C_B , and the transition rates are determined by linear fitting. Specifically, $k_{AB} = 1.3485 \times 10^{-2}$, $\tilde{k}_{AB} = 1.3707 \times 10^{-2}$, $k_{BA} = 1.3836 \times 10^{-2}$, $\tilde{k}_{BA} = 1.3656 \times 10^{-2}$. The errors of transition rates between the trajectory data and the trajectories generated by the RC-NF model are both less than 0.001. From the perspective of transition rate, we can declare that the RC-NF model successfully reproduces the original stochastic DW system.

The RC-NF model can be successfully employed for DW systems, whether from the perspective of probability density function or transition rate. In other words, RC-NF could serve as a surrogate model

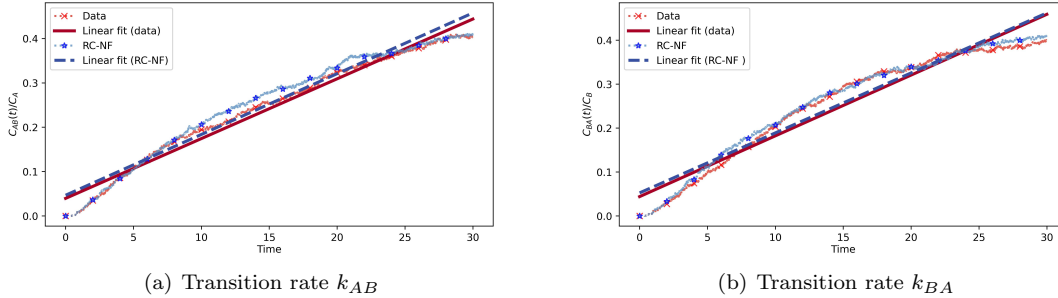


Figure 5: Transition rates (a) k_{AB} and (b) k_{BA} are obtained by trajectory data and RC-NF model generating trajectories. The red cross-dot lines are calculated from trajectory data, and the linear fitting produces the solid red lines. The blue asterisk dot lines are calculated from the RC-NF generating trajectories, while linear fitting produces the dashed blue lines.

for analyzing stochastic DW systems, allowing for a deeper understanding of their internal mechanisms and enabling early warning of rare events or critical transition phenomena.

4.3 Linear SDDE: long-term prediction of a non-Markov process

The aforementioned systems (Sec. 4.1, Sec. 4.2) are stationary and Markov processes. Stochastic processes arising from solutions of SDDEs (3) typically lack the Markov property. As we mentioned in Sec. 2.2, various data-driven approaches have been proposed for the analysis of stochastic dynamical systems. However, due to the complexity of the system and specific model assumptions, most existing methods cannot be extended to analyze SDDEs from data. At present, there is relatively little research on this type of system. First, we consider the following SDDE with a linear coefficient [3]:

$$\begin{cases} dX_t = \mu_0 X_{t-\tau_0} dt + g dB_t, & \text{for } t \geq 0, \\ X_t = t + 1, & \text{for } t \in [-\tau_0, 0], \end{cases} \quad (22)$$

where $\mu_0 \in \mathbb{R}$, time delay $\tau_0 > 0$, the diffusion coefficient g is a positive constant, and B_t is a scalar Brownian motion. We take $\mu_0 = -1.2$, $\tau_0 = 1$, $g = 1$, and the existence of the solution of the above SDDE (22) is guaranteed [3]. Based on the above parameter assumptions, we use the Itô formula to obtain the solution on the time interval $[0, 2]$:

$$X_t = \begin{cases} 1 - 0.6t^2 + B_t, & \text{for } t \in [0, 1], \\ 0.2(t-1)^2 - t + 1.4 + \int_1^t B_{s-1} ds + B_t, & \text{for } t \in [1, 2]. \end{cases} \quad (23)$$

Note that although this linear SDDE (22) is formally similar to the OU process (18), their solutions are significantly different from each other.

For this system, we follow the time step setting from the previous examples, that is, $\delta t = \Delta t = 0.01$. The initial value is $X_0 = 1$, which is determined by equation (22). We generate 2000 trajectories with a total length of 2000 using the Euler-Maruyama scheme, where the training length T , verification length T_{valid} , and prediction length T_{test} are 1000, 100, and 900 respectively, and the first 100 steps of training are used for warm-up.

The results of rolling predictions of the RC-NF model are shown in Fig. 6. Fig. 6(a) depicts the probability density functions of the trajectory data and the rolling predictions of RC-NF on the test dataset. The results of RC-NF rolling predictions mimic the fluctuation of the probability density function over time. Fig. 6(b) displays Wasserstein distances and KL divergences at different times t ; the red dashed lines represent the selected snapshots, and their probability density functions and specific values are displayed in Fig. 6(c) and Tables 2 and 3, respectively. These results demonstrate the efficiency of the RC-NF model we proposed and its ability to predict the non-Markov linear SDDE over the long term.

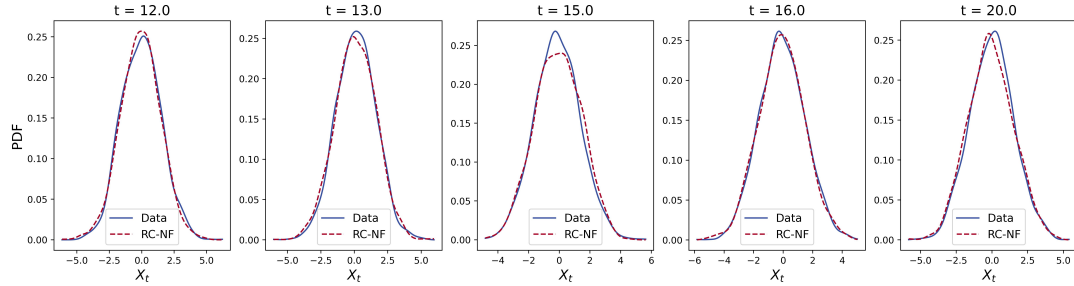
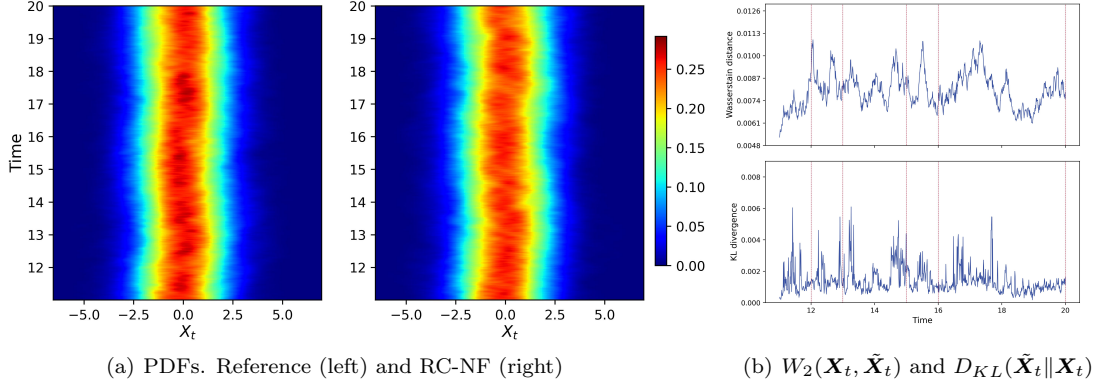


Figure 6: Results of the linear SDDE. PDFs of the trajectory data and the RC-NF rolling predictions are shown in (a). (b) Wasserstein distance (top) and KL divergence (bottom), the red dashed lines represent snapshots where we draw the PDFs in (c) and display the values in Tables 2 and 3.

Although it is a simple linear SDDE (22), it differs significantly from the previous two examples (OU process, DW system) defined by SDEs. However, our proposed RC-NF achieves almost the same level of accuracy in predicting the long-term evolution of the linear SDDE.

4.4 El Niño Southern Oscillation (ENSO) simplified model

Consider the simplified El Niño Southern Oscillation (ENSO) model [56, 57] with additive noise that is presented below,

$$\begin{cases} dX_t = (X_t - X_t^3 - \alpha_0 X_{t-\tau_0})dt + g dB_t, & \text{for } t \geq 0, \\ X_t = C_0, & \text{for } t \in [-\tau_0, 0], \end{cases} \quad (24)$$

where $|\alpha_0| < 1$ measures the influence of the returning signal relative to that of the local feedback, τ_0 is the time delay corresponding to wave transit time, the constant $C_0 \in \mathbb{R}$, the diffusion coefficient g is also a positive constant, and B_t is a scalar Brownian motion. Note that the deterministic model corresponding to (24) has two stable fixed points at $X_t = (1 - \alpha_0)^{1/2}$ and $X_t = -(1 - \alpha_0)^{1/2}$, and one unstable fixed point at $X_t = 0$. In accordance with [56, 57], we set $\alpha_0 = 0.75$ and $\tau_0 = 6$.

For this system, we follow the time step setting from the previous examples, that is, $\delta t = \Delta t = 0.01$. The initial values $X_0 = C_0$, C_0 are drawn from a uniform distribution on $[-1, 1]$. We generate 2000 trajectories with a total length of 4000 using the Euler-Maruyama scheme, where the training length T , verification length T_{valid} , and prediction length T_{test} are 2000, 100, and 1900 respectively, and the first 100 steps of training are used for warm-up.

Noting that the probability distribution of state X_t of this system depends on the initial value C_0 , we fix the initial value $X_0 = -0.1$ and use the trained RC-NF model to generate new trajectories to explore the performance of the proposed method. A small piece of data of length $T_{warm} = 500$ is

used to warm up, and 2000 trajectories are generated by the Euler-Maruyama scheme and the trained RC-NF model, respectively.

The comparison results of the trajectory data and the trajectories generated by the RC-NF model are shown in Fig. 7. More specifically, Fig. 7(a) depicts the probability density functions of the trajectory data and trajectories generated by the RC-NF model. As can be seen from the figure, the RC-NF model successfully captures the change in probability density over time, with its highest peak alternating with time. Fig. 7(b) displays Wasserstein distances and KL divergences at different times t ; the red dashed lines represent the selected snapshots, and their probability density functions and specific values are displayed in Fig. 7(c) and Tables 2 and 3, respectively. Although there is a slight difference in peaks, we have been successful in learning the bimodal probability density function of the system at a fixed time. Although the transition rate k_{AB} is no longer approximately constant for $\tau_{mol} < t \ll \tau_{rxn}$, as shown in Sec. 4.2, we can still calculate the time correlation function $C_{AB}(t)/C_A$ to assess the quality of the RC-NF model, the relevant results are shown in Fig. 7(d). Time correlation functions of trajectory data and of the trajectories generated by the RC-NF model have roughly the same trend. For the ESNO simplified model (24), the proposed method is still effective.

The ESNO simplified model is the most complex one-dimensional stochastic dynamical system we consider in this article, whose corresponding SDDE (24) is nonlinear, and the solution of the SDDE is a non-Markov, non-stationary stochastic process. Its evolution depends on initial values and time delay. Nevertheless, RC-NF successfully predicts the evolution of state variables in the probability distribution sense within the tolerable error and remains competitive in some qualitative and quantitative analyses.

4.5 Stochastic Lorenz system: further comparison of RC and RC-NF

Lorenz system [58] is notable for having chaotic solutions depending on the parameter values and starting conditions. This demonstrates how physically deterministic systems can still have some inherent unpredictability. Moreover, the necessity of stochasticity in the climate system and some related studies can be found in [59–61]. One of the stochastic forms of Lorenz system describes by the following nonlinear SDEs:

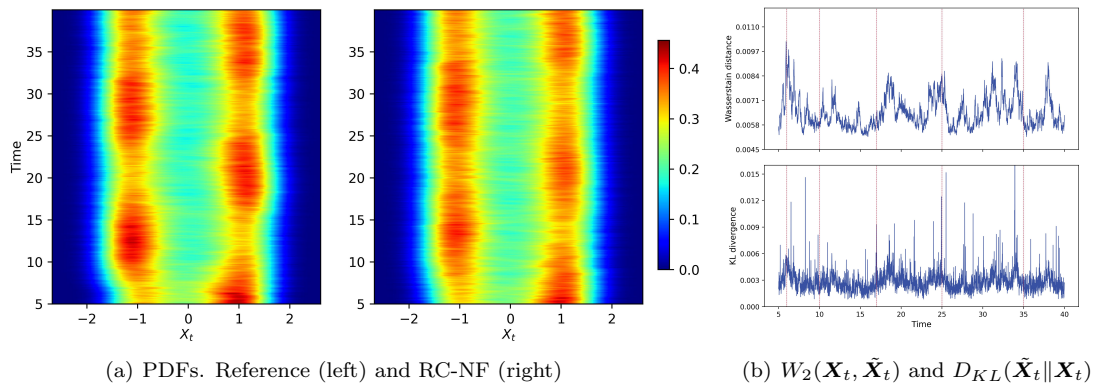
$$\begin{cases} dX_t = \sigma_0(Y_t - X_t)dt + g^1 dB_t^1, \\ dY_t = (X_t(\rho_0 - Z_t) - Y_t)dt + g^2 dB_t^2, \\ dZ_t = (X_t Y_t - \beta_0 Z_t)dt + g^3 dB_t^3, \end{cases} \quad (25)$$

where g^1, g^2, g^3 are positive constants on the diagonal of the diffusion coefficient matrix \mathbf{g} and $[B_t^1, B_t^2, B_t^3]^T$ is a three-dimensional standard Brownian Motion. The control parameters are the Prandtl Number σ_0 , the Rayleigh Number ρ_0 , and a domain geometric factor β_0 . We select $\sigma_0 = 10$, $\rho_0 = 28$, $\beta = 8/3$, and $g^1 = g^2 = g^3 = 3$.

For this system, we set the time step of the Euler-Maruyama scheme $\delta t = 10^{-5}$ and the observation step $\Delta t = 0.01$. The initial value is $[X_0, Y_0, Z_0]^T = [0, 1, 0]^T$. We generate 1000 trajectories with a total length of 4000 using the Euler-Maruyama scheme, where the training length T , validation length T_{valid} , and prediction length T_{test} are 2000, 100, and 1900 respectively, and the first 100 steps of training are used for warm-up. The generated sample trajectories are standardized, i.e., $X_t^{(m)}(\text{new}) = (X_t^{(m)} - \text{Mean}_{t,m}(X_t^{(m)})) / \text{Std}_{t,m}(X_t^{(m)})$, and $Y_t^{(m)}(\text{new})$ and $Z_t^{(m)}(\text{new})$ are dealt with in similar ways.

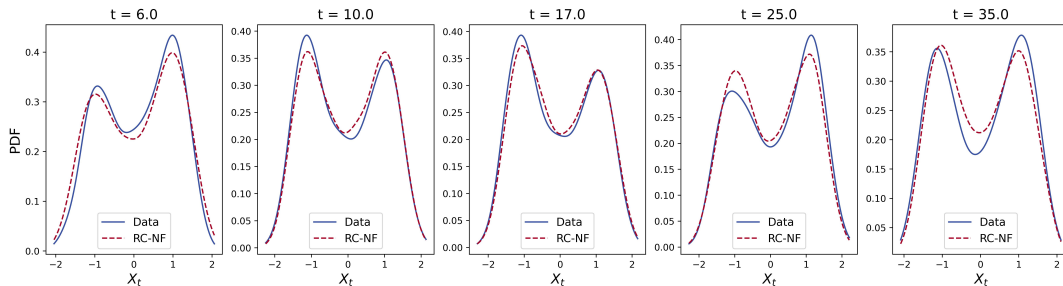
RC can also replicate the strange attractor of the Lorenz system, so the main task of this subsection is to compare the performance of RC and RC-NF in the stochastic Lorenz system. We first plot the trajectory data in the testing phase, the trajectories predicted by the RC model, and the trajectories predicted by the RC-NF model in three-dimensional space, as shown in Fig. 8(a). Unsurprisingly, the trajectories of all three exhibit butterfly-like strange attractors. Fig. 8(b) depicts the probability density functions of the trajectory data and the rolling predictions of RC and RC-NF on the test dataset. The prediction results of RC-NF and the results of the trajectory data are similar, but the prediction results of RC are quite different, although it exhibits a butterfly-like strange attractor. Due to the ergodicity of the Lorenz system, we calculate the Wasserstein distance and KL divergence between the datasets (trajectory data, rolling predictions of RC model, rolling predictions of RC-NF model) composed of all states in testing as shown in Table 4. Results from RC-NF outperform to those from RC.

We use two criteria to further characterize the difference between RC and RC-NF to highlight the excellent performance of RC-NF. The metric approach is maximum Lyapunov exponents [25, 62, 63]

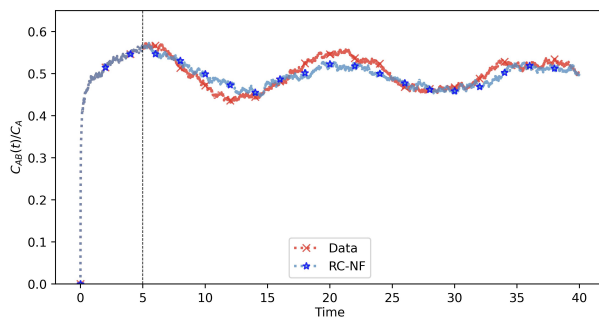


(a) PDFs. Reference (left) and RC-NF (right)

(b) $W_2(\mathbf{X}_t, \tilde{\mathbf{X}}_t)$ and $D_{KL}(\tilde{\mathbf{X}}_t \parallel \mathbf{X}_t)$



(c) PDFs. Reference (solid blue lines) and RC-NF results (red dashed lines) for several snapshots selected on the test dataset



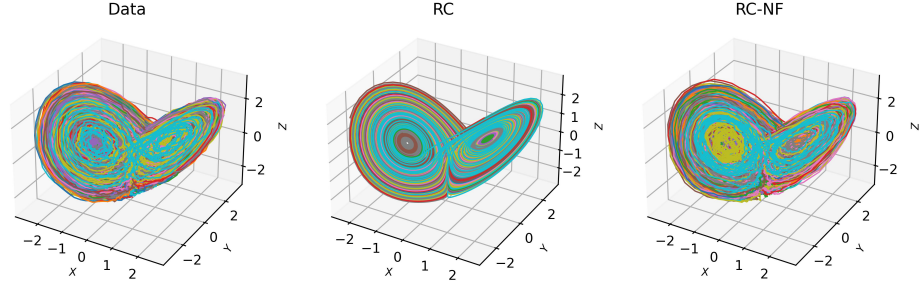
(d) Time correlation function $C_{AB}(t)$

Figure 7: Comparison results of ENSO simplified model. PDFs of the trajectory data and the RC-NF rolling predictions are shown in (a). (b) Wasserstein distance (top) and KL divergence (bottom) at different times t , the red dashed lines represent snapshots where we draw the PDFs in (c) and display the values in Tables 2 and 3. (d) Time correlation function $C_{AB}(t)$, the red cross dot line is calculated from the trajectory data, and the blue asterisk line is calculated from trajectories generated by the RC-NF model. The black dotted line represents the split between warm-up and generation.

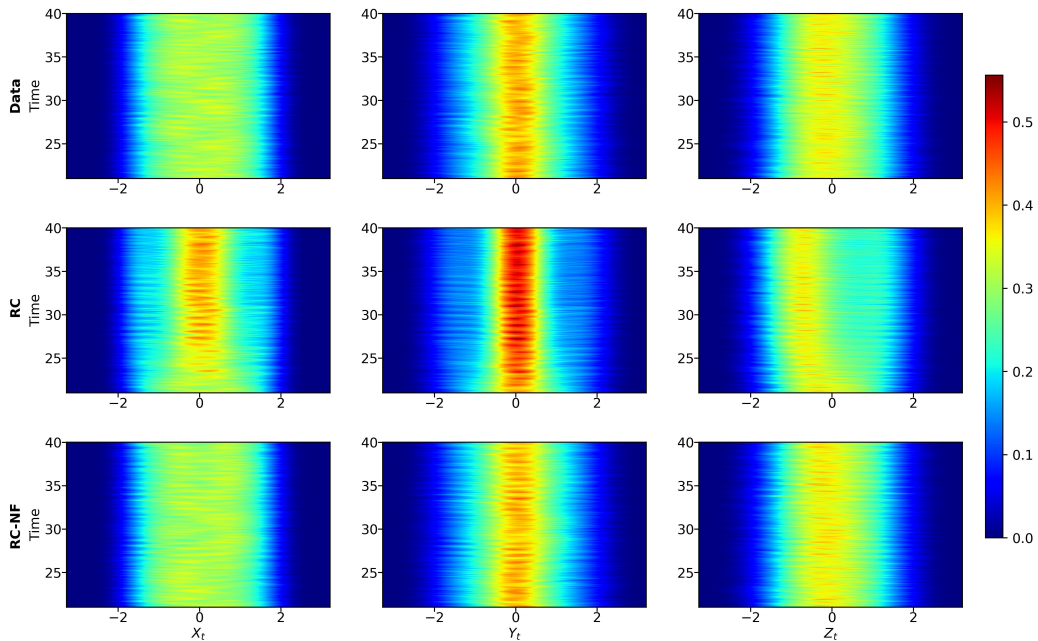
Table 4: Stochastic Lorenz model: Wasserstein distances and KL divergences are calculated for RC and RC-NF predictions, respectively.

Criteria	RC	RC-NF
Wasserstein distance	4.7918×10^{-2}	2.6603×10^{-2}
KL divergence	4.6666×10^{-4}	7.5146×10^{-5}

and the topological approach is close returns [60, 64]. The Lyapunov exponent of a dynamical system is a quantity that characterizes how quickly two infinitesimally similar trajectories separate from one



(a) Trajectories in testing, data (left), generated by RC (middle), generated by RC-NF (right)



(b) Marginal PDFs. References (top), RC (middle), and RC-NF (bottom)

Figure 8: Data, rolling predictions of RC and RC-NF on the test dataset for stochastic Lorenz system. (a) Strange attractors; (b) PDFs in the testing phase.

another. The largest one is called the maximal Lyapunov exponent (MLE). A positive MLE is typically seen as a criterion of chaos in the system. Using the technique described in [62], MLEs are computed for each trajectory in testing. The trajectory data and the trajectories predicted by the RC model and the RC-NF model are shown in the form of boxplots in Fig. 9(a). Similar to the results of the probability density functions, the boxplot of the trajectory data is consistent with the prediction results of the RC-NF model, which shows that their MLEs are close. Note that the median of MLEs of the RC model is 1.8525, it is also no longer consistent with the MLE of the noiseless Lorenz system under our parameter settings (MLE= 0.91).

Close returns are used to identify segments in the chaotic time series that can stand in for the unstable periodic orbits that surround the strange attractor. For a trajectory $\mathbf{X}_{T+T_{valid}+t}$, $t = 1, \dots, T_{test}$ on the test dataset, close returns segments can be identified in the data by making a two-dimensional

close returns plot of

$$\|\mathbf{X}_t - \mathbf{X}_{t+p}\|_2 \begin{cases} < \varepsilon_0, & \text{black,} \\ > \varepsilon_0, & \text{white,} \end{cases} \quad (26)$$

where lag $p > 0$, and $\varepsilon_0 > 0$ is a fixed threshold depending on the diameter of the attractor, $\varepsilon_0 \sim 10^{-2} \times (\text{Max}(\mathbf{X}_t) - \text{Min}(\mathbf{X}_t))$. We can draw a two-dimensional binary image of (t, p) . Considering our testing settings, we set $t = 1, \dots, 1000$ and $p = 1, \dots, 900$. A arbitrarily selected trajectory on the test dataset is used to draw close returns maps of the trajectory data, RC prediction results, and RC-NF prediction results in Fig. 9(c). There are few differences in close returns maps among the three. Fig. 9(b) is histograms of p formed by the black pixels of all predicted trajectories. Again, the peak positions and heights of the RC-NF prediction results match the trajectory data, while RC can only match a few peak positions.

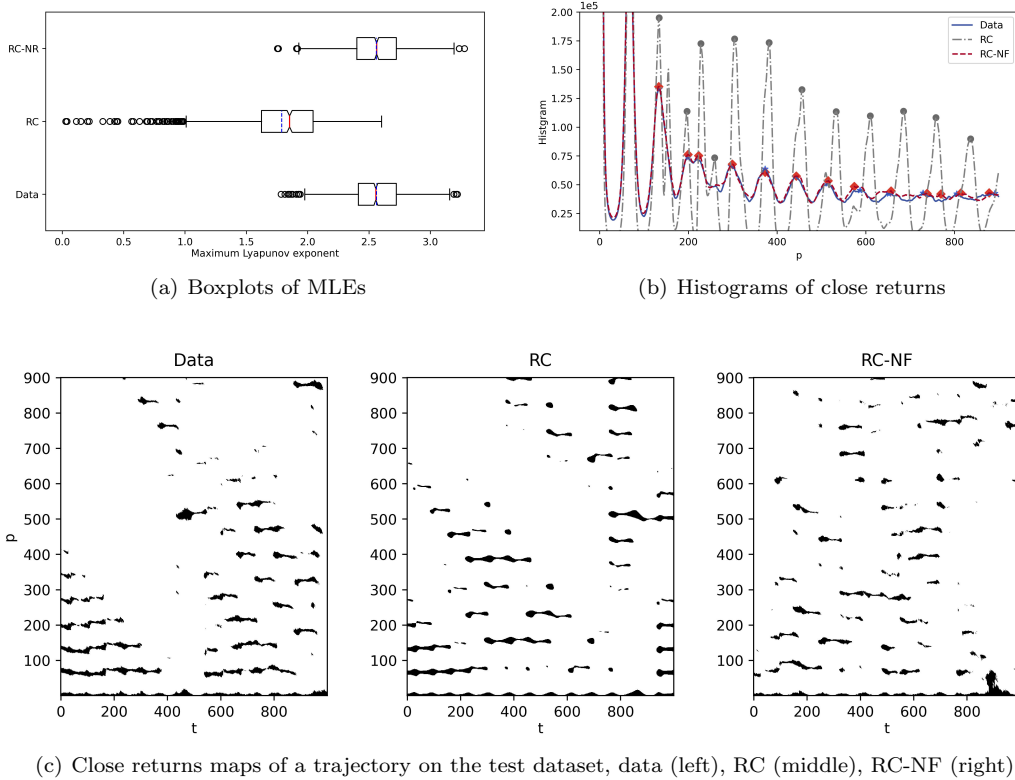


Figure 9: Criteria of stochastic Lorenz systems. (a) Boxplots composed of MLEs of multiple trajectories. The red solid lines represent the medians of MLEs, and the blue dashed lines represent the means of MLEs. Medians: 2.5557 (data), 1.8525 (RC), 2.5622 (RC-NF). Means: 2.5609 (data), 1.7881 (RC), 2.5592 (RC-NF). (b) Close returns histograms. The solid blue line is derived from the trajectory data, the gray dotted line is derived from the RC prediction result, the red dashed line is derived from the RC-NF prediction result, and their peaks are also marked with various markers. (c) Close returns maps of a trajectory in the testing phase.

We use the Euler-Maruyama scheme (time step $\delta t = 10^{-5}$), the RC model, and the RC-NF model to generate a long trajectory with the length of 10^6 and observation time step $\Delta t = 0.01$, respectively. The warm-up time for RC and RC-NF models is $T_{warm} = 500$. The probability density functions, autocorrelation functions (ACFs) and cross-correlation functions (CCFs) are compared using the long trajectories generated by the three methods, the results are shown in Fig. 10. For these long trajectories, as depicted in Fig. 10(a), the marginal probability density functions of the three dimensions indicate that the trajectory generated by the RC-NF model is closer to the trajectory generated by the numerical scheme, while the trajectory generated by RC is significantly different. The cross-correlation function between sequences X and Y is a deterministic function of lag p defined as

$r_p^{XY} = \text{Mean}_t((X_t - \bar{X})(Y_{t+p} - \bar{Y})) / \sqrt{\text{Std}_t(X_t) \cdot \text{Std}_t(Y_t)}$, where \bar{X} and \bar{Y} represent the means of sequences X and Y . In general, $r_p^{XY} \neq r_p^{YX}$, and r_p^{XX} represents the ACF of sequence X . ACFs and CCFs of three long trajectories generated by different methods can be found in Fig. 10(b). It is also clear that the results of the RC-NF model are closer to those of the numerical scheme.

In summary, for the stochastic Lorenz system, we investigate its capacity to replicate strange attractors, the evolution of probability density, MLEs, and close returns maps on the test dataset. When comparing a long trajectory generated by different methods, we display the probability density functions, ACFs, and CCFs. RC-NF exhibits overwhelming advantages over traditional RC.

5 Discussion

In this paper, we devise a novel approach to predict the long-term evolution of stochastic dynamical systems and capture the corresponding dynamical behaviors. The framework (shorten as RC-NF) we proposed is model-free and takes only a few assumptions about the underlying stochastic dynamical systems (the approach is valid for SDEs/SDDEs, and it may be generalized to more types of systems). RC-NF combines the benefits of Reservoir Computing for long-term prediction, as well as Normalizing Flow for producing samples from an approximated error distribution, both with low computational costs. We also illustrate the universality of the proposed framework under the discrete-time setting.

We verify the effectiveness of our framework with five examples: the Ornstein-Uhlenbeck process, Double-Well system, linear SDDE, ENSO simplified model, and stochastic Lorenz system. Multiple criteria are reused in prediction tasks and generation tasks to manifest the effectiveness of RC-NF, namely, the probability density function, Wasserstein distance, KL divergence, transition rate, maximum Lyapunov exponent, close returns, autocorrelation function and cross-correlation function.

Despite the success of RC-NF, there are several directions that might be further explored. We shall extend the applicability of RC-NF to multiplicative noise or non-Gaussian noise to accommodate more complex systems [1], which also implies a relaxation of Assumption 1. More kinds of dynamical behaviors or transition dynamics, such as stable/unstable/center manifolds, intermittency, bifurcation-induced tipplings, and rate-induced tipplings [7], should be investigated. Moreover, we have not taken into consideration of more complicated RC frameworks, such as next generation reservoir computing [27], Deep reservoir computing [38], etc, whose efficiency is uncertain yet.

CRedit authorship contribution statement

Cheng Fang: Conceptualization, Methodology, Software, Formal analysis, Writing - Original Draft. **Yubin Lu:** Conceptualization, Methodology, Formal analysis, Writing - Original Draft. **Ting Gao:** Conceptualization, Methodology, Funding acquisition, Writing - Review & Editing. **Jinqiao Duan:** Discussion, Funding acquisition.

Declaration of competing interest

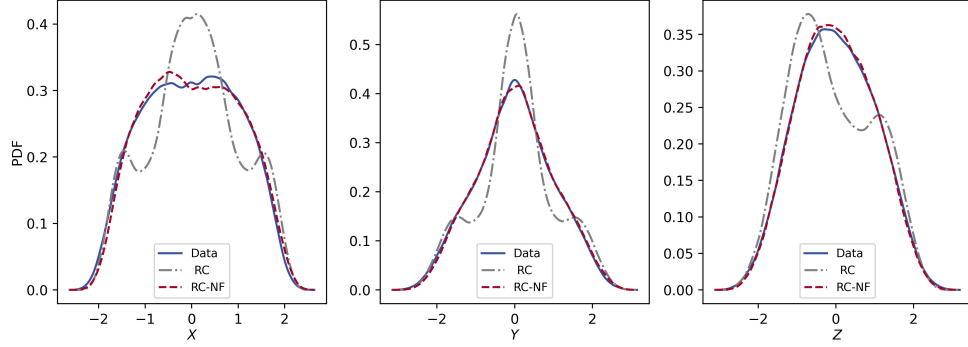
The authors declare that they have no known competing financial interests or personal relationships that could have appeared to influence the work reported in this paper.

Data availability

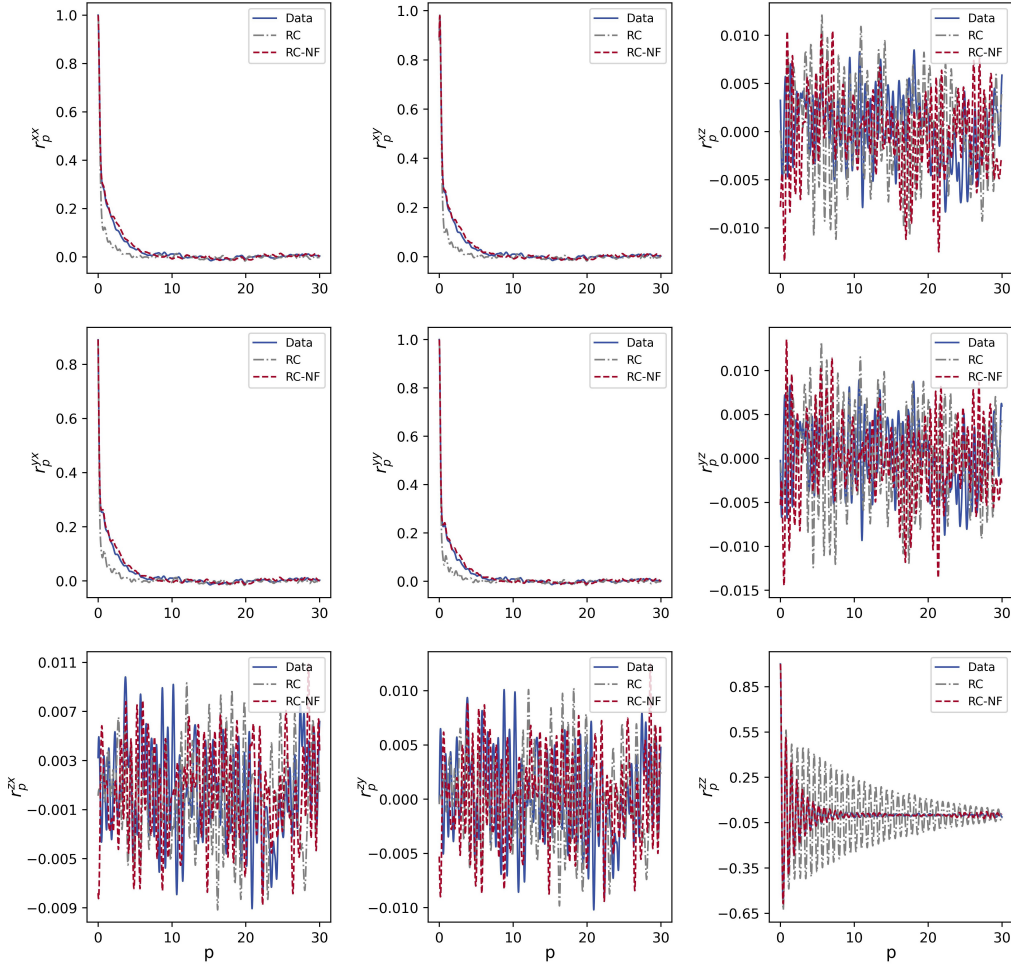
No data was used for the research described in the article. The code that supports the paper’s findings can be found in GitHub <https://github.com/Fangransto/RC-NF>.

Acknowledgements

We would like to thank Xu Sun, Ting Li, Wei Wei, and Luxuan Yang for helpful discussions. This work was supported by the National Key Research and Development Program of China 2021ZD0201300, the National Natural Science Foundation of China 12141107, and Fundamental Research Funds for



(a) Marginal PDFs of a long trajectory



(b) ACFs (on the diagonal) and CCFs (off the diagonal) of a long trajectory

Figure 10: Results of a long trajectory. (a) Marginal PDFs. (b) ACFs and CCFs. The blue solid lines are the results of the trajectory generated by the numerical scheme, the gray dotted lines are the results of the trajectory generated by the RC model, and the red dashed lines are the results of the trajectory generated by the RC-NF model.

the Central Universities 5003011053. Lu was partially supported by the grant DOE DE-SC00222766 and NSF-2216926.

Appendix A Universality theory supplement

In this section we supplement the theory required for the universality of Reservoir Computing, as well as the proofs of Theorem 1 and Theorem 2.

The following theorem proves the universality of ESN (16) in the L^p -sense.

Lemma A1. (Gonon and Ortega [36], Theorem 2) Fix $p \in [1, \infty)$, let \mathbf{Z} be a fixed \mathbb{R}^d -valued input process, and let H be a functional such that $H(\mathbf{Z}) \in L^p(\Omega, \mathcal{F}, \mathbb{P})$. Suppose that the activation function $\sigma : \mathbb{R} \rightarrow \mathbb{R}$ is nonconstant, continuous, and has a bounded image. Then for any $\varepsilon > 0$, there exists $N \in \mathbb{N}$, $W_{in} \in \mathbb{M}_{N,d}$, $\boldsymbol{\zeta} \in \mathbb{R}^d$, $A \in \mathbb{M}_N$, $\mathbf{w} \in \mathbb{R}^N$ such that (16) has the ESP, the corresponding filter is causal and time-invariant, the associated functional satisfies $H_{\mathbf{w}}^{A, W_{in}, \boldsymbol{\zeta}}(\mathbf{Z}) \in L^p(\Omega, \mathcal{F}, \mathbb{P})$ and

$$\|H(\mathbf{Z}) - H_{\mathbf{w}}^{A, W_{in}, \boldsymbol{\zeta}}(\mathbf{Z})\|_p < \varepsilon. \quad (\text{A1})$$

Remark A1. The image of a filter map U is a one-dimensional discrete time series. By stacking d filters U^i , $i = 1, 2, \dots, d$, we can create a d -dimensional filter $\mathbf{U} : ((\mathbb{R}^d)^{\mathbb{Z}}, \otimes_{t \in \mathbb{Z}} \mathcal{B}(\mathbb{R}^d)) \rightarrow ((\mathbb{R}^d)^{\mathbb{Z}}, \otimes_{t \in \mathbb{Z}} \mathcal{B}(\mathbb{R}^d))$. Additionally, by repeatedly utilizing Lemma A1, it is possible to create a d -dimensional \mathbf{U}' whose components satisfy (16).

Based on the above Lemma A1, we show that if the time delay operator is bounded, then filters of the form (16) are identical in the L^p -sense when the input sequences can be represented by each other using time delay operators.

Theorem 1. Let U be a causal and time-invariant filter and its associated functional is H . Fix $p \in [1, \infty)$, let \mathbf{Z} be a fixed \mathbb{R}^d -valued input process, and $H(\pi_{\mathbb{Z}_-}(\mathbf{Z})) \in L^p(\Omega, \mathcal{F}, \mathbb{P})$. Assume the time delay operator T_{-s} is a bounded operator for any $s \in \mathbb{Z}$. Then there exists causal and time-invariant filters U' , $U^{s'}$ satisfying (16), constructed by input sequences $\pi_{\mathbb{Z}_-}(\mathbf{Z})$, $\pi_{\mathbb{Z}_-} \circ T_{-s}(\mathbf{Z})$, respectively, that are identical in the L^p -sense. That is, $\|U'(\mathbf{Z})_s - U^{s'}(\mathbf{Z})_s\|_p < (\|T_{-s}\|_p + 1)\varepsilon$.

Proof. Without losing the generality, we consider the bounded time delay operator T_{-1} . Denote $\mathbf{Z}^{(1)} = (\dots, \mathbf{Z}_{-1}, \mathbf{Z}_0) \in ((\mathbb{R}^d)^{\mathbb{Z}_-}, \otimes_{t \in \mathbb{Z}_-} \mathcal{B}(\mathbb{R}^d))$, $\mathbf{Z}^{(2)} = (\dots, \mathbf{Z}_{-1}, \mathbf{Z}_0, \mathbf{Z}_1) \in ((\mathbb{R}^d)^{\mathbb{Z}}, \otimes_{t \in \mathbb{Z}} \mathcal{B}(\mathbb{R}^d))$, we have $\mathbf{Z}^{(2)} = T_{-1}(\mathbf{Z}^{(1)})$. Due to the boundedness of T_{-1} , $H(\mathbf{Z}^{(2)}) \in L^p(\Omega, \mathcal{F}, \mathbb{P})$.

Using Lemma A1, for any $\varepsilon > 0$, there exists causal and time-invariant filters of the form (16) and associated functionals for input sequences $\mathbf{Z}^{(1)}$ and $\mathbf{Z}^{(2)}$, denoted as U' and H' , U'' and H'' , respectively. In particular, for arbitrary $\varepsilon > 0$, $\|H(\mathbf{Z}^{(1)}) - H'(\mathbf{Z}^{(1)})\|_p < \varepsilon$, $\|H(\mathbf{Z}^{(2)}) - H''(\mathbf{Z}^{(2)})\|_p < \varepsilon$. Hence, for input sequence $\mathbf{Z}^{(2)}$,

$$\begin{aligned} & \|H'(\mathbf{Z}^{(2)}) - H''(\mathbf{Z}^{(2)})\|_p \\ &= \|H'(\mathbf{Z}^{(2)}) - H(\mathbf{Z}^{(2)}) + H(\mathbf{Z}^{(2)}) - H''(\mathbf{Z}^{(2)})\|_p \\ &\leq \|H'(\mathbf{Z}^{(2)}) - H(\mathbf{Z}^{(2)})\|_p + \|H(\mathbf{Z}^{(2)}) - H''(\mathbf{Z}^{(2)})\|_p \\ &= \|H'(T_{-1}(\mathbf{Z}^{(1)})) - H(T_{-1}(\mathbf{Z}^{(1)}))\|_p + \|H(\mathbf{Z}^{(2)}) - H''(\mathbf{Z}^{(2)})\|_p \\ &= \|U'(T_{-1}(\mathbf{Z}^{(1)}))_0 - U(T_{-1}(\mathbf{Z}^{(1)}))_0\|_p + \|H(\mathbf{Z}^{(2)}) - H''(\mathbf{Z}^{(2)})\|_p \\ &= \|T_{-1}(U'(\mathbf{Z}^{(1)}))_0 - T_{-1}(U(\mathbf{Z}^{(1)}))_0\|_p + \|H(\mathbf{Z}^{(2)}) - H''(\mathbf{Z}^{(2)})\|_p \\ &\leq \|T_{-1}\|_p \| (U'(\mathbf{Z}^{(1)}))_0 - (U(\mathbf{Z}^{(1)}))_0 \|_p + \|H(\mathbf{Z}^{(2)}) - H''(\mathbf{Z}^{(2)})\|_p \\ &= \|T_{-1}\|_p \|H'(\mathbf{Z}^{(1)}) - H(\mathbf{Z}^{(1)})\|_p + \|H(\mathbf{Z}^{(2)}) - H''(\mathbf{Z}^{(2)})\|_p \\ &< (\|T_{-1}\|_p + 1)\varepsilon, \end{aligned}$$

which is equivalent to $\|U'(\mathbf{Z}^{(2)})_0 - U''(\mathbf{Z}^{(2)})_0\|_p < (\|T_{-1}\|_p + 1)\varepsilon$. For any $s \in \mathbb{Z}$, $\mathbf{Z}^{(s)}$ can be constructed similarly such that $\|U'(\mathbf{Z}^{(s)})_0 - U^{s'}(\mathbf{Z}^{(s)})_0\|_p < (\|T_{-s}\|_p + 1)\varepsilon$. More generally, $\|U'(\mathbf{Z})_s - U^{s'}(\mathbf{Z})_s\|_p < (\|T_{-s}\|_p + 1)\varepsilon$ for any $s \in \mathbb{Z}$. The required result follows due to the arbitrariness of ε . \square

We generalize the conclusions of Lemma A1 and Theorem 1 to discrete time series $(\mathbf{X}_t^{\delta t})_{t \in \mathbb{Z}}$ based on the numerical scheme.

Theorem 2. Define a filter $\mathbf{U} : ((\mathbb{R}^d)^{\mathbb{Z}}, \otimes_{t \in \mathbb{Z}} \mathcal{B}(\mathbb{R}^d)) \rightarrow ((\mathbb{R}^d)^{\mathbb{Z}}, \otimes_{t \in \mathbb{Z}} \mathcal{B}(\mathbb{R}^d))$ by $\mathbf{U}((\mathbf{X}_t^{\delta t})_{t \in \mathbb{Z}})_t = \mathbf{X}_{t+1}^{\delta t}$. Let $(\mathbf{X}_t^{\delta t})^{(1)} := (\dots, \mathbf{X}_{t-1}^{\delta t}, \mathbf{X}_t^{\delta t})$ be a fixed \mathbb{R}^d -valued input process. Then for arbitrary $\varepsilon > 0$, there

exists $N \in \mathbb{N}$, $W_{in} \in \mathbb{M}_{N,d}$, $\zeta \in \mathbb{R}^d$, $A \in \mathbb{M}_N$, $\mathbf{w} \in \mathbb{R}^N$ such that (16) has the ESP, the corresponding filter is causal and time-invariant, the associated functional satisfies $\mathbf{H}_{\mathbf{w}}^{A,W_{in},\zeta}((\mathbf{X}_t^{\delta t})^{(1)}) \in L^2(\Omega, \mathcal{F}, \mathbb{P})$ and

$$\|\mathbf{H}((\mathbf{X}_t^{\delta t})^{(1)}) - \mathbf{H}_{\mathbf{w}}^{A,W_{in},\zeta}((\mathbf{X}_t^{\delta t})^{(1)})\|_2 < \varepsilon. \quad (\text{A2})$$

Additionally, for any $s \in \mathbb{Z}$, consider input sequences $(\mathbf{X}_t^{\delta t})^{(1)}$ and $T_{-s}((\mathbf{X}_t^{\delta t})^{(1)})$, there exists causal and time-invariant filters $U', U^{s'}$ satisfying (16), constructed by input sequences $(\mathbf{X}_t^{\delta t})^{(1)}$, $T_{-s}((\mathbf{X}_t^{\delta t})^{(1)})$, that are identical in the L^2 -sense.

Proof. Let's consider that the dimension of X is 1, and the d -dimension case can be easily generalized by Remark A1. For the filter U defined in Theorem 2, the associated functional is $H((X_t^{\delta t})^{(1)}) := U((X_t^{\delta t})^{(1)})_0 = X_{t+1}^{\delta t} \in L^2(\Omega, \mathcal{F}, \mathbb{P})$. Then the formula (A2) is obtained by Lemma A1.

For any $s \in \mathbb{Z}$, we have $T_{-s}(X_t^{\delta t}) = X_{t+s}^{\delta t} \in L^2(\Omega, \mathcal{F}, \mathbb{P})$, which means that T_{-s} is a bounded operator. The required result follows by utilizing Theorem 1. \square

A.1 The difference between RC and ESN on linear SDDE

We use the linear SDDE mentioned in Sec. 4.3 to prove the difference between RC (4), (6) and ESN (16). The specific settings are identical to those in Sec. 4.3, with the exception that the ESN framework is simpler and does not require the selection of hyperparameter α . We show some results that differ significantly between the two.

The mean of Wasserstein distance of the ESN-NF method during the testing phase is 8.0540×10^{-3} , whereas the RC-NF method is 7.9967×10^{-3} . During the test period, the mean of KL divergence of the ESN-NF method in testing is 1.7927×10^{-3} , while the RC-NF method is 1.4012×10^{-3} . By imitating Fig. 2 in Sec. 4.1, we depict the rolling prediction results of the ESN-NF method and RC-NF method in Fig. A1.

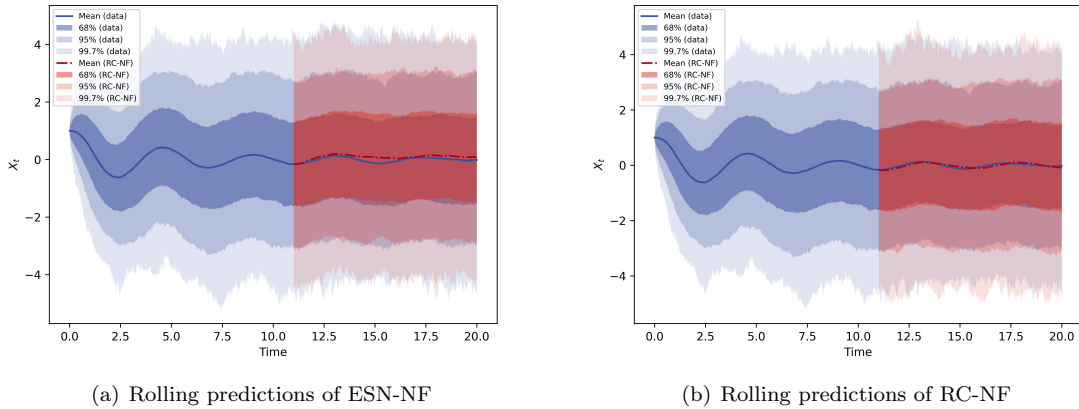


Figure A1: Rolling predictions of ESN-NF and RC-NF. The solid blue line denotes the sample mean, and the shaded blue portions from dark to light represent the intervals calculated from the trajectory data. Rolling predictions using ESN-NF and RC-NF produce the red dotted dashes and shaded areas. (a) Rolling predictions of ESN-NF; (b) Rolling predictions of RC-NF.

Results-wise, the rolling prediction results of RC-NF are slightly superior to those of ESN-NF. It is undeniable that both theory and experiment show that ESN can indeed achieve good prediction results, while RC makes the prediction effect better.

Appendix B Hyperparameters of various experiments

We initialize the Bayesian Optimization search process with the provided initial parameters and set the number of iterations to 50. After 50 iterations, the hyperparameters of RC corresponding to the smallest \mathcal{L}_2 error selected by BO on the validation dataset are shown in Table B1.

Table B1: The optimal hyperparameters selected by the Bayesian Optimization algorithm in each example.

Experiments	ρ	k	χ	α	λ
OU process	0.5173	3	0.8933	0.8570	1.0000×10^0
DW system	0.8609	3	1.3469	0.9839	5.7206×10^{-2}
Linear SDDE	0.9324	4	0.3655	0.2008	2.2073×10^{-6}
ESNO simplified model	0.8654	1	0.6024	0.0500	5.0616×10^{-5}
stochastic Lorenz system	0.3972	5	0.3817	0.9694	7.7623×10^{-2}

References

- [1] Jinqiao Duan. *An introduction to stochastic dynamics*, volume 51. Cambridge University Press, 2015.
- [2] Xuerong Mao. *Stochastic differential equations and applications*. Elsevier, 2007.
- [3] Fathalla A. Rihan. *Delay differential equations and applications to biology*. Springer, 2021.
- [4] Peter H. Baxendale and Sergey V. Lototsky. *Stochastic differential equations: theory and applications*, volume 2. World Scientific, 2007.
- [5] Weinan E, Tiejun Li, and Eric Vanden-Eijnden. *Applied stochastic analysis*, volume 199. American Mathematical Soc., 2021.
- [6] Steven H. Strogatz. *Nonlinear dynamics and chaos: With applications to physics, biology, chemistry, and engineering*. CRC press, 2015.
- [7] Peter Ashwin, Sebastian Wieczorek, Renato Vitolo, and Peter Cox. Tipping points in open systems: bifurcation, noise-induced and rate-dependent examples in the climate system. *Philosophical Transactions of the Royal Society A: Mathematical, Physical and Engineering Sciences*, 370(1962):1166–1184, 2012.
- [8] Stefan Klus, Feliks Nüske, Sebastian Peitz, Jan-Hendrik Niemann, Cecilia Clementi, and Christof Schütte. Data-driven approximation of the koopman generator: Model reduction, system identification, and control. *Physica D: Nonlinear Phenomena*, 406:132416, 2020.
- [9] Yubin Lu and Jinqiao Duan. Discovering transition phenomena from data of stochastic dynamical systems with lévy noise. *Chaos: An Interdisciplinary Journal of Nonlinear Science*, 30(9), 09 2020. 093110.
- [10] Lorenzo Boninsegna, Feliks Nüske, and Cecilia Clementi. Sparse learning of stochastic dynamical equations. *The Journal of Chemical Physics*, 148(24), 03 2018. 241723.
- [11] Yubin Lu, Yang Li, and Jinqiao Duan. Extracting stochastic governing laws by non-local kramers–moyal formulae. *Philosophical Transactions of the Royal Society A*, 380(2229):20210195, 2022.
- [12] Felix Dietrich, Alexei Makeev, George Kevrekidis, Nikolaos Evangelou, Tom Bertalan, Sebastian Reich, and Ioannis G. Kevrekidis. Learning effective stochastic differential equations from microscopic simulations: Linking stochastic numerics to deep learning. *Chaos: An Interdisciplinary Journal of Nonlinear Science*, 33(2), 02 2023. 023121.
- [13] Cheng Fang, Yubin Lu, Ting Gao, and Jinqiao Duan. An end-to-end deep learning approach for extracting stochastic dynamical systems with α -stable Lévy noise. *Chaos: An Interdisciplinary Journal of Nonlinear Science*, 32(6), 06 2022. 063112.
- [14] Xiaoli Chen, Liu Yang, Jinqiao Duan, and George Em Karniadakis. Solving inverse stochastic problems from discrete particle observations using the fokker–planck equation and physics-informed neural networks. *SIAM Journal on Scientific Computing*, 43(3):B811–B830, 2021.

- [15] Xiaoli Chen, Hui Wang, and Jinqiao Duan. Detecting stochastic governing laws with observation on stationary distributions. *Physica D: Nonlinear Phenomena*, 448:133691, 2023.
- [16] Yubin Lu, Romit Maulik, Ting Gao, Felix Dietrich, Ioannis G. Kevrekidis, and Jinqiao Duan. Learning the temporal evolution of multivariate densities via normalizing flows. *Chaos: An Interdisciplinary Journal of Nonlinear Science*, 32(3), 03 2022. 033121.
- [17] John Harlim, Shixiao W. Jiang, Senwei Liang, and Haizhao Yang. Machine learning for prediction with missing dynamics. *Journal of Computational Physics*, 428:109922, 2021.
- [18] Xuechen Li, Ting-Kam Leonard Wong, Ricky T.Q. Chen, and David K. Duvenaud. Scalable gradients and variational inference for stochastic differential equations. In *Symposium on Advances in Approximate Bayesian Inference*, pages 1–28. PMLR, 2020.
- [19] Yuanran Zhu, Yu-Hang Tang, and Changho Kim. Learning stochastic dynamics with statistics-informed neural network. *Journal of Computational Physics*, 474:111819, 2023.
- [20] Kohei Nakajima and Ingo Fischer. *Reservoir computing: Theory, Physical Implementations, and Applications*. Springer Singapore, 2021.
- [21] Herbert Jaeger and Harald Haas. Harnessing nonlinearity: Predicting chaotic systems and saving energy in wireless communication. *Science*, 304(5667):78–80, 2004.
- [22] Wolfgang Maass, Thomas Natschläger, and Henry Markram. Real-time computing without stable states: A new framework for neural computation based on perturbations. *Neural computation*, 14(11):2531–2560, 2002.
- [23] Wolfgang Maass. Liquid state machines: motivation, theory, and applications. *Computability in context: computation and logic in the real world*, pages 275–296, 2011.
- [24] Jan Yperman and Thijs Becker. Bayesian optimization of hyper-parameters in reservoir computing. *arXiv preprint arXiv:1611.05193*, 2016.
- [25] Jaideep Pathak, Brian Hunt, Michelle Girvan, Zhixin Lu, and Edward Ott. Model-free prediction of large spatiotemporally chaotic systems from data: A reservoir computing approach. *Phys. Rev. Lett.*, 120:024102, Jan 2018.
- [26] Aaron Griffith, Andrew Pomerance, and Daniel J. Gauthier. Forecasting chaotic systems with very low connectivity reservoir computers. *Chaos: An Interdisciplinary Journal of Nonlinear Science*, 29(12), 12 2019. 123108.
- [27] Daniel J. Gauthier, Erik Bollt, Aaron Griffith, and Wendson A.S. Barbosa. Next generation reservoir computing. *Nature communications*, 12(1):5564, 2021.
- [28] Mousumi Roy, Swarnendu Mandal, Chittaranjan Hens, Awadhesh Prasad, N. V. Kuznetsov, and Manish Dev Shrimali. Model-free prediction of multistability using echo state network. *Chaos: An Interdisciplinary Journal of Nonlinear Science*, 32(10), 10 2022. 101104.
- [29] Dagobert Wenkack Liedji, Jimmi Hervé Talla Mbé, and Godpromesse Kenne. Classification of hyperchaotic, chaotic, and regular signals using single nonlinear node delay-based reservoir computers. *Chaos: An Interdisciplinary Journal of Nonlinear Science*, 32(12), 12 2022. 123126.
- [30] Daniel J. Gauthier, Ingo Fischer, and André Röhm. Learning unseen coexisting attractors. *Chaos: An Interdisciplinary Journal of Nonlinear Science*, 32(11), 11 2022. 113107.
- [31] Soon Hoe Lim, Ludovico Theo Giorgini, Woosok Moon, and J. S. Wettlaufer. Predicting critical transitions in multiscale dynamical systems using reservoir computing. *Chaos: An Interdisciplinary Journal of Nonlinear Science*, 30(12), 12 2020. 123126.
- [32] Dhruvit Patel, Daniel Canaday, Michelle Girvan, Andrew Pomerance, and Edward Ott. Using machine learning to predict statistical properties of non-stationary dynamical processes: System climate, regime transitions, and the effect of stochasticity. *Chaos: An Interdisciplinary Journal of Nonlinear Science*, 31(3), 03 2021. 033149.

- [33] Dhruvit Patel and Edward Ott. Using machine learning to anticipate tipping points and extrapolate to post-tipping dynamics of non-stationary dynamical systems. *Chaos: An Interdisciplinary Journal of Nonlinear Science*, 33(2), 02 2023. 023143.
- [34] Herbert Jaeger, Mantas Lukoševičius, Dan Popovici, and Udo Siewert. Optimization and applications of echo state networks with leaky-integrator neurons. *Neural Networks*, 20(3):335–352, 2007. Echo State Networks and Liquid State Machines.
- [35] Izzet B. Yildiz, Herbert Jaeger, and Stefan J. Kiebel. Re-visiting the echo state property. *Neural networks*, 35:1–9, 2012.
- [36] Lukas Gonon and Juan-Pablo Ortega. Reservoir computing universality with stochastic inputs. *IEEE Transactions on Neural Networks and Learning Systems*, 31(1):100–112, 2020.
- [37] Lukas Gonon and Juan-Pablo Ortega. Fading memory echo state networks are universal. *Neural Networks*, 138:10–13, 2021.
- [38] Claudio Gallicchio, Alessio Micheli, and Luca Pedrelli. Deep reservoir computing: A critical experimental analysis. *Neurocomputing*, 268:87–99, 2017. Advances in artificial neural networks, machine learning and computational intelligence.
- [39] Gouhei Tanaka, Toshiyuki Yamane, Jean Benoit Héroux, Ryosho Nakane, Naoki Kanazawa, Seiji Takeda, Hidetoshi Numata, Daiju Nakano, and Akira Hirose. Recent advances in physical reservoir computing: A review. *Neural Networks*, 115:100–123, 2019.
- [40] Georg A. Gottwald and Sebastian Reich. Supervised learning from noisy observations: Combining machine-learning techniques with data assimilation. *Physica D: Nonlinear Phenomena*, 423:132911, 2021.
- [41] Matthew Levine and Andrew Stuart. A framework for machine learning of model error in dynamical systems. *Communications of the American Mathematical Society*, 2(07):283–344, 2022.
- [42] Ian Goodfellow, Jean Pouget-Abadie, Mehdi Mirza, Bing Xu, David Warde-Farley, Sherjil Ozair, Aaron Courville, and Yoshua Bengio. Generative adversarial nets. In *Advances in Neural Information Processing Systems*, volume 27, pages 2672–2680. Curran Associates, Inc., 2014.
- [43] Diederik P. Kingma and Max Welling. Auto-Encoding Variational Bayes. In *2nd International Conference on Learning Representations, ICLR 2014, Banff, AB, Canada, April 14-16, 2014, Conference Track Proceedings*, 2014.
- [44] Jonathan Ho, Ajay Jain, and Pieter Abbeel. Denoising diffusion probabilistic models. *Advances in Neural Information Processing Systems*, 33:6840–6851, 2020.
- [45] Conor Durkan, Artur Bekasov, Iain Murray, and George Papamakarios. Neural spline flows. In H. Wallach, H. Larochelle, A. Beygelzimer, F. d'Alché-Buc, E. Fox, and R. Garnett, editors, *Advances in Neural Information Processing Systems*, volume 32. Curran Associates, Inc., 2019.
- [46] George Papamakarios, Eric Nalisnick, Danilo Jimenez Rezende, Shakir Mohamed, and Balaji Lakshminarayanan. Normalizing flows for probabilistic modeling and inference. *The Journal of Machine Learning Research*, 22(1):2617–2680, 2021.
- [47] Ivan Kobyzev, Simon J.D. Prince, and Marcus A. Brubaker. Normalizing flows: An introduction and review of current methods. *IEEE Transactions on Pattern Analysis and Machine Intelligence*, 43(11):3964–3979, 2021.
- [48] I. A. Khovanov. Stochastic approach for assessing the predictability of chaotic time series using reservoir computing. *Chaos: An Interdisciplinary Journal of Nonlinear Science*, 31(8), 08 2021. 083105.
- [49] Zhiqiang Liao, Zeyu Wang, Hiroyasu Yamahara, and Hitoshi Tabata. Low-power-consumption physical reservoir computing model based on overdamped bistable stochastic resonance system. *Neurocomputing*, 468:137–147, 2022.

- [50] Ali Rodan and Peter Tino. Minimum complexity echo state network. *IEEE Transactions on Neural Networks*, 22(1):131–144, 2011.
- [51] Pauliina Kärkkäinen and Riku Linna. The optimal reservoir computer for nonlinear dynamics. *arXiv preprint arXiv:2202.05159*, 2022.
- [52] R. E. Kalman. A New Approach to Linear Filtering and Prediction Problems. *Journal of Basic Engineering*, 82(1):35–45, 03 1960.
- [53] Stephen Boyd and Leon O. Chua. Fading memory and the problem of approximating nonlinear operators with volterra series. *IEEE Transactions on Circuits and Systems*, 32(11):1150–1161, 1985.
- [54] Chin-Wei Huang, David Krueger, Alexandre Lacoste, and Aaron Courville. Neural autoregressive flows. In *International Conference on Machine Learning*, pages 2078–2087. PMLR, 2018.
- [55] Peter G. Bolhuis, David Chandler, Christoph Dellago, and Phillip L. Geissler. Transition path sampling: Throwing ropes over rough mountain passes, in the dark. *Annual Review of Physical Chemistry*, 53(1):291–318, 2002. PMID: 11972010.
- [56] Max J. Suarez and Paul S. Schopf. A delayed action oscillator for enso. *Journal of Atmospheric Sciences*, 45(21):3283–3287, 1988.
- [57] Xu Sun and Fang Yang. Time evolution of probability density in stochastic dynamical systems with time delays: The governing equation and its numerical solution. *Chaos: An Interdisciplinary Journal of Nonlinear Science*, 32(12), 12 2022. 123124.
- [58] Edward N. Lorenz. Deterministic nonperiodic flow. *Journal of Atmospheric Sciences*, 20(2):130–141, 1963.
- [59] T.N. Palmer. Stochastic weather and climate models. *Nature Reviews Physics*, 1(7):463–471, 2019.
- [60] Sahil Agarwal and J.S. Wettlaufer. Maximal stochastic transport in the lorenz equations. *Physics Letters A*, 380(1):142–146, 2016.
- [61] Tapio Schneider, Andrew M Stuart, and Jin-Long Wu. Learning stochastic closures using ensemble Kalman inversion. *Transactions of Mathematics and Its Applications*, 5(1), 12 2021. tnab003.
- [62] Michael T. Rosenstein, James J. Collins, and Carlo J. De Luca. A practical method for calculating largest lyapunov exponents from small data sets. *Physica D: Nonlinear Phenomena*, 65(1-2):117–134, 1993.
- [63] Jaideep Pathak, Zhixin Lu, Brian R. Hunt, Michelle Girvan, and Edward Ott. Using machine learning to replicate chaotic attractors and calculate lyapunov exponents from data. *Chaos: An Interdisciplinary Journal of Nonlinear Science*, 27(12), 12 2017. 121102.
- [64] Gabriel M. Mindlin and R. Gilmore. Topological analysis and synthesis of chaotic time series. *Physica D: Nonlinear Phenomena*, 58(1):229–242, 1992.